ACS Biomaterials SCIENCE & ENGINEERING

Article

pubs.acs.org/journal/abseba

Fatty Acid-Mimetic Micelles for Dual Delivery of Antigens and Imidazoquinoline Adjuvants

Sema Sevimli,[†] Frances C. Knight,[‡] Pavlo Gilchuk,[§,∥] Sebastian Joyce,[§,∥,⊥] and John T. Wilson*[,†,‡,⊥]

[†]Department of Chemical and Biomolecular Engineering, Vanderbilt University, 2400 Highland Avenue, Nashville, Tennessee 37235, United States

[‡]Department of Biomedical Engineering, Vanderbilt University, 2301 Vanderbilt Place, Nashville, Tennessee 37235, United States

[§]Department of Pathology, Microbiology and Immunology, Vanderbilt University School of Medicine, Medical Center North, Nashville, Tennessee 37232, United States

[∥]Department of Veterans Administration Tennessee Valley Healthcare System, 1310 24th Avenue South, Nashville, Tennessee 37212, United States

[⊥]Vanderbilt Center for Immunobiology, Vanderbilt University Medical Center, 2301 Vanderbilt Place, Nashville, Tennessee 37235, United States

Supporting Information

ABSTRACT: Vaccine design has undergone a shift toward the use of purified protein subunit vaccines, which offer increased safety and greater control over antigen specificity, but at the expense of immunogenicity. Here we report the development of a new polymer-based vaccine delivery platform engineered to enhance immunity through the codelivery of protein antigens and the Toll-like receptor 7 (TLR7) agonist imiquimod (IMQ). Because of the preferential solubility of IMQ in fatty acids, a series of block copolymer micelles with a fatty acid-mimetic core comprising lauryl methacrylate (LMA) and methacrylic acid (MAA), and a poly(ethylene glycol) methyl ether methacrylate (PEGMA) corona decorated with pyridyl disulfide ethyl methacrylate (PDSM) moieties for antigen conjugation were synthesized via reversible addition−fragmentation chain transfer (RAFT) polymerization. Carriers composed of 50 mol % LMA (LMA50) demonstrated the highest IMQ loading (2.2 w/w%) and significantly enhanced the immunostimulatory capacity of IMQ to induce dendritic cell maturation and proinflammatory cytokine production. Conjugation of a model antigen, ovalbumin (OVA), to the corona of IMQ-loaded LMA50 micelles enhanced in vitro antigen uptake and cross-presentation on MHC class I (MHC-I). A single intranasal (i.n.) immunization of mice with carriers coloaded with IMQ and OVA elicited significantly higher pulmonary and systemic $CD8^+$ T cell responses and increased serum IgG titer relative to a soluble formulation of antigen and adjuvant. Collectively, these data demonstrate that rationally designed fatty acid-mimetic micelles enhance intracellular antigen and IMQ delivery, and have potential as synthetic vectors for enhancing the immunogenicity of subunit vaccines.

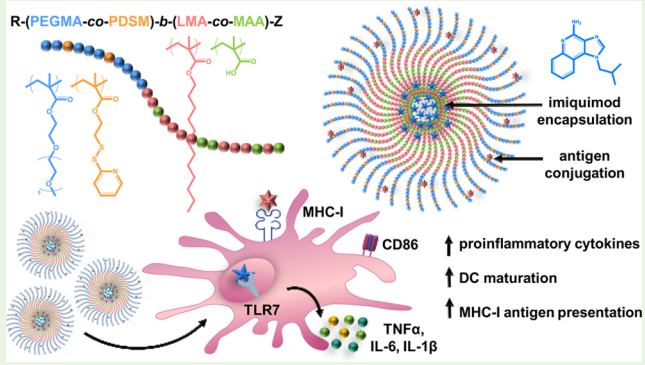

KEYWORDS: *imiquimod, subunit vaccine, block copolymer micelles, RAFT polymerization, Toll-like receptor 7, mucosal immunity*

INTRODUCTION

The development of vaccines and universal implementation of vaccinations has eliminated or dramatically reduced the global burden of infectious disease. Nevertheless, there remains an urgent and unmet need for effective vaccines against many diseases (e.g., malaria, tuberculosis, and human immunodeficiency virus) that have proven recalcitrant to traditional vaccine design approaches.[1,2] Toward this end, vaccine development is shifting away from organism-based vaccines toward microbial peptide/protein subunit vaccines that confer greater control over antigen-specificity of the immune response while offering increased safety.[2] Subunit vaccines tend to demonstrate poor immunogenicity and, therefore, must be delivered with immunostimulatory adjuvants to increase vaccine potency.[3−5] Most currently clinically approved adjuvants (e.g., alum) primarily elicit humoral immune responses, with minimal induction of cellular immunity.[6] In particular, current Food and Drug Administration (FDA)-approved adjuvants poorly elicit $CD8^+$ cytotoxic T cell and Th1 $CD4^+$ responses that are critical

Special Issue: Biomaterials for Immunoengineering

Received: July 20, 2016
Accepted: November 9, 2016
Published: November 9, 2016

DOI: 10.1021/acsbiomaterials.6b00408
ACS Biomater. Sci. Eng. 2017, 3, 179−194

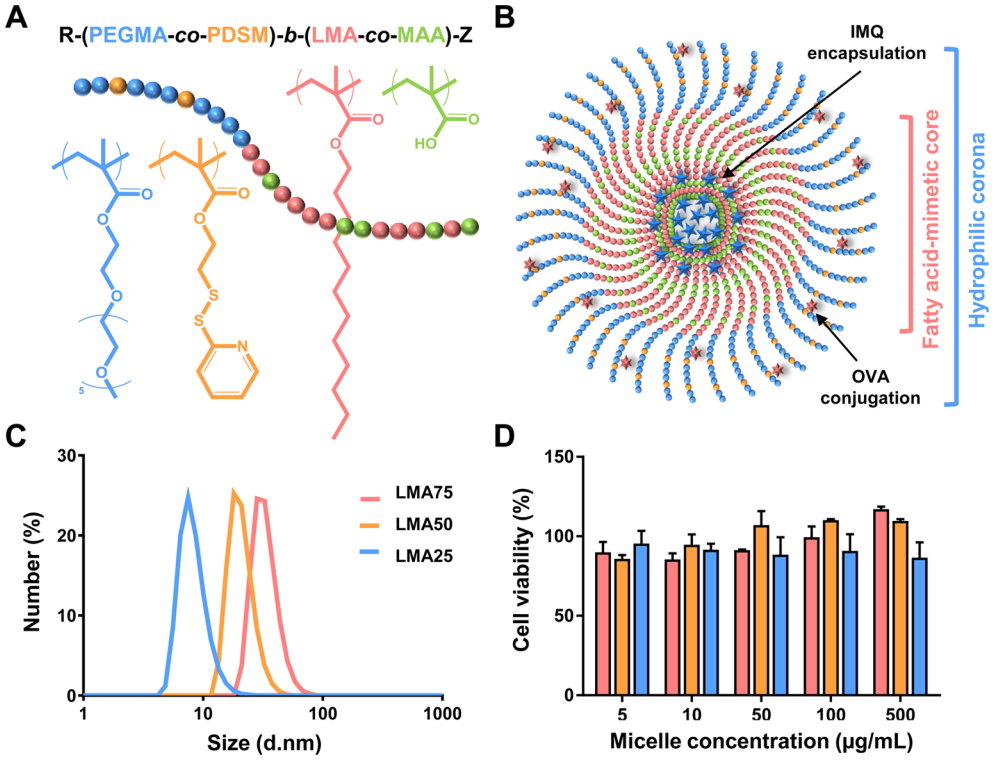

Figure 1. Fatty acid-mimetic micelles for dual delivery of antigen and adjuvant. (A) P(PEGMA-*co*-PDSM)-*b*-(LMA-*co*-MAA) polymers with varying LMA composition were synthesized via RAFT polymerization. (B) The hydrophilic shell was composed of PEGMA and a small percentage of thiol-reactive PDSM for the conjugation of antigens. The hydrophobic and fatty acid-mimetic core comprising LMA and MAA drives micelle assembly, creating an optimal environment for IMQ loading. (C) Representative size distribution (number-average) measured via DLS of LMA75, LMA50, and LMA25. (D) Representative cell viability of BMDCs after incubation with P(PEGMA-*co*-PDSM)-*b*-(LMA-*co*-MAA) micelles for 24 h as measured with Alamar Blue assay. The assay was repeated three times in 4 replicates and the viability results were normalized according to the control treatment (untreated cells). Error bars represents standard deviation.

for protection against a number of important intracellular pathogens, including malaria, tuberculosis, and viruses.[3,7,8]

Modern vaccine design is guided by the principle that the innate immune response to a pathogen significantly influences the quality, magnitude, breadth, and longevity of the resultant adaptive immune response.[3,4,9,10] The innate immune response to pathogens is triggered by pattern-recognition receptors (PRRs) that recognize pathogen-associated molecular patterns (PAMPs).[11] Understanding these interactions has informed the rational design of PRR agonists that are under intensive investigation as vaccine adjuvants to promote cellular immunity, including a growing number of Toll-like receptor (TLR) agonists.[12] TLRs are a set of conserved PRRs responsible for sensing microbial pathogens and are primarily expressed by immune cells such as macrophages, neutrophils, B cells, and dendritic cells (DCs). In general, TLR agonists enhance subunit vaccine immunogenicity by promoting antigen presentation, increasing costimulatory molecule expression, and stimulating production of inflammatory cytokines that together drive T cell activation and differentiation.[13] In addition to their use as vaccine adjuvants, a number of TLR agonists have been included in the National Cancer Institute's list of immunotherapeutic agents for their potential in treating cancer.[14]

TLR7 is localized in endosomal membranes and is involved in recognition of single-stranded RNA generated during viral infection.[15] Activation of TLR7 induces a MyD88-dependent signaling cascade, ultimately leading to the secretion of inflammatory cytokines such as tumor necrosis factor (TNF) α, type I interferons (i.e., IFN-α and IFN-β), and interleukin (IL)-12 that promote T cell immunity.[16] Imiquimod (IMQ) is a synthetic imidazoquinoline and small molecule TLR7 agonist that has been widely explored as an adjuvant to improve the efficacy of subunit vaccines,[17−19] and is FDA-approved in a topical formulation (Aldara, 3M) for the treatment of genital warts, superficial basal cell carcinoma, actinic keratosis, and melanoma.[20] However, the low aqueous solubility of IMQ imposes significant formulation challenges that have restricted its use to topical applications.[21] Moreover, IMQ and structurally related imidazoquinoline compounds with higher aqueous solubility (e.g., resiquimod and gardiquimod) diffuse rapidly after administration with minimal accumulation in draining lymph nodes.[18,22−24] These unfavorable physicochemical and pharmacokinetic properties reduce the efficacy of IMQ as a vaccine adjuvant and can give rise to systemic inflammation and toxic side effects.[25−27]

These challenges motivate the design of particle-based delivery systems for IMQ and other small molecule TLR7/8 agonists that can extend half-life,[18] reduce systemic distribution,[23,28] enhance uptake by antigen presenting cells (APCs),[29−31] and/or promote accumulation and/or retention in tumors and/or lymph nodes.[18,32] Moreover, for vaccine applications, dual delivery of protein antigens and TLR agonists,[18,33−35] including IMQ,[30,36,37] on a single carrier can further potentiate immune responses by increasing the probability that antigen and TLR agonist reach the same antigen presenting cell. To date, most approaches for IMQ delivery have utilized emulsified polymeric micro- and nanoparticles to encapsulate IMQ in a degradable matrix (e.g.,

DOI: 10.1021/acsbiomaterials.6b00408
ACS Biomater. Sci. Eng. 2017, 3, 179−194

PLGA particles).[29−32,38] These approaches can suffer from low IMQ loading, burstlike release kinetics, and particle sizes greater than 200 nm that do not efficiently harness lymphatic trafficking to increase uptake in draining lymph nodes[39] nor accumulate in tumors via the enhanced permeability and retention (EPR) effect.[40] Moreover, for vaccine applications, particle fabrication often exposes antigens to organic solvents and harsh processing conditions that can degrade or denature subunit antigens.[41] These limitations have prompted exploration of alternative carrier systems (e.g., liposomes, cubosomes, chitosan nanocapsules)[36,37,42] and approaches for delivery of IMQ and other small molecule TLR7/8 agonists, including recent pioneering work by the Seder and De Geest groups on covalent ligation of novel, but non-FDA approved, imidazoquinolines to polymeric carriers.[18,23] In the present study, we describe the rational design of sub-100 nm polymer nanoparticles for dual delivery of IMQ and protein subunit antigens.

Unlike most hydrophobic compounds for which polymeric delivery systems have been developed (e.g., paclitaxel), IMQ also has low solubility in most common organic solvents (e.g., chloroform, methanol, acetone), which imposes unique challenges for carrier development. Nonetheless, IMQ is highly soluble in many fatty acids;[21] indeed, isostearic acid acts as the primary solubilizing agent in the topical formulation Aldara. Hence, we hypothesized that synthetic polymers mimicking the structure of fatty acids - fatty acid-mimetic - designed to form micellar nanoparticles will enhance IMQ solubility and delivery (Figure 1A-B). Here we describe a new class of vaccine carrier composed of a hydrophilic poly(ethylene glycol) methyl ether methacrylate (PEGMA) corona featuring pyridyl disulfide methacrylate (PDSM) functionalities for the conjugation of thiolated-antigens,[33,43−45] and a fatty acid-mimetic core containing lauryl methacrylate (LMA) and methacrylic acid (MAA) for encapsulation of IMQ. Reversible addition−fragmentation chain transfer (RAFT) polymerization[46,47] was used to synthesize a series of (PEGMA-*co*-PDSM)-*block*-(LMA-*co*-MAA) copolymers, and the effect of second block composition on micellar self-assembly, IMQ encapsulation, drug release kinetics, and immunostimulatory activity was explored. These investigations unveiled a window in copolymer composition in which a balance of hydrophobic and acidic monomers enabled efficient IMQ loading into charge-neutral, highly PEGylated, 30 nm particles that facilitated enhanced TLR7 activation in vitro. Pendant PDSM groups in the hydrophilic micelle corona were exploited for covalent conjugation of protein antigen via a reducible disulfide bond, facilitating dual delivery of IMQ and subunit antigens. Finally, we demonstrate the ability of this subunit vaccine platform to enhance murine antigen-specific pulmonary and systemic $CD8^+$ T cell immune responses, as well as humoral responses, using a needle-free, intranasal delivery route.

MATERIALS AND METHODS

RAFT Synthesis of P(PEGMA-*co*-PDSM)-*b*-(LMA-*co*-MAA). A series of poly(poly(ethylene glycol) methyl ether methacrylate-*co*-pyridyldisulfide ethyl methacrylate)-*block*-(lauryl methacrylate-*co*-methacrylic acid) (P(PEGMA-*co*-PDSM)-*b*-(LMA-*co*-MAA)) block copolymers with LMA content of 25, 50, and 75 mol % was synthesized via RAFT polymerization. PDSM monomer was synthesized according to the procedure reported in the literature with minor modifications (Scheme S1 and Figure S1, Supporting Information)[48,49] and commercial monomers (PEGMA M_n 300 g/mol, LMA, *tert*-butyl methacrylate (*t*-BMA), Sigma-Aldrich) were purified via basic alumina gel column chromatography prior to use.

A P(PEGMA-*co*-PDSM) macroRAFT chain transfer agent (CTA) was synthesized at a molar ratio of 100:1:0.2 representing total monomer, CTA, and initiator ratios, respectively. In brief, 6.2 g of PEGMA (20 mmol), 460 mg of PDSM (1.8 mmol), 62 mg of RAFT agent 4-(cyanopentanoic acid)-4-dithiobenzoate (CPADB; 0.22 mmol, Sigma-Aldrich), and 7.4 mg of initiator 2,2-azobis(isobutyronitrile) (AIBN; 0.04 mmol, recrystallized twice from methanol prior to use, Sigma-Aldrich) were dissolved in 45 mL of anhydrous toluene, sealed with a rubber septa and purged with $N_2(g)$ for 30 min on ice. The mixture was polymerized at 70 °C for 6 h. The crude mixture was analyzed by ^{1}H NMR ($CDCl_3$) to determine conversion from the monomeric vinyl peaks (-C═$\underline{CH_2}$, δ = 6.2−5.6) and the PEGMA O-$\underline{CH_2}CH_2$ peak (δ = 4.2) (DP_n:36). The polymer was purified by precipitating the crude product into cold pentane (4×) and vacuum drying overnight. The composition and molecular weight of the purified macroRAFT was obtained by ^{1}H NMR (Figure S2) and gel permeation chromatography (GPC, Agilent; mobile phase HPLC-grade dimethylformamide (DMF) containing 0.1% LiBr), respectively. Molecular weight and polydispersity indices (PDI) were calculated using the ASTRA V Software (Wyatt Technology).

^{1}H NMR ($CDCl_3$, 400 MHz in ppm): 8.46 (1H, aromatic proton ortho-N), 7.68 (2H, aromatic proton meta-N and para-N), 7.12 (1H, aromatic proton, orthodisulfide linkage), 4.19 (2H, -S-S-$CH_2\underline{CH_2}$O-), 4.06 (2H, -O-$\underline{CH_2}CH_2$-), 3.63 (12H, -O-($\underline{CH_2}\underline{CH_2}$-O)$_n$), 3.53 (2H, -O-$CH_2\underline{CH_2}$-), 3.36 (3H, CH_2-O-$\underline{CH_3}$-), 3.03 (2H, -S-S-$\underline{CH_2}CH_2$O−-), 1.01 (3H, methyl proton of the methacryloyl group), 0.86 (3H, -C-$\underline{CH_3}$)

The macroRAFT CTA was chain extended with LMA and *t*-BMA monomers followed by acid hydrolysis of the *tert*-butyl group to form fatty-acid mimetic block copolymers with varying LMA composition (25, 50, and 75 mol % LMA, described herein as LMA25, LMA50, and LMA75, respectively). A representative polymerization (LMA25) consisted of the dissolution of LMA (0.25 g, 1 mmol), *t*-BMA (0.42 g, 3 mmol), macroRAFT (440 mg, 0.04 mmol), and AIBN (1.32 mg, 0.008 mmol) in anhydrous toluene (2 mL). The mixture was purged with $N_2(g)$ for 30 min on ice and reacted for 9 h at 70 °C. The resultant diblock copolymer was purified by membrane dialysis (Snakeskin dialysis tubing MWCO 3500, Thermo Scientific) against acetone:water (Ace:H_2O 80:20 v/v, water ratio was increased each day) for 3 days followed by lyophilization and analyzed via ^{1}H NMR (Figure S3) and GPC.

^{1}H NMR ($CDCl_3$, 400 MHz in ppm): 3.93 (2H, -O-$\underline{CH_2}CH_2$-), 1.57 (2H, -O-$CH_2\underline{CH_2}$-), 1.41 (9H, -C-($\underline{CH_3}$)$_3$), 1.25 (18H, CH_2-($\underline{CH_2}$)$_6$-CH_3), 1.02 (3H, -C-$\underline{CH_3}$), 0.87 (3H, -C-$\underline{CH_3}$)

P(PEGMA-*co*-PDSM)-*b*-(LMA_{25}-*co*-*t*-BMA_{75}) (370 mg, 1.96 mmol *tert*-butyl ester) was dissolved in dichloromethane (DCM; 4.1 mL). The diblock copolymer was dissolved for 10 min followed by dropwise addition of trifluoroacetic acid (TFA; 0.747 mL, 9.77 mmol) under vigorous stirring. The reaction continued to stir for 30 h at RT. Excess TFA and DCM were removed via rotary evaporation and deprotected polymer was dried under vacuum overnight. Removal of *tert*-butyl group from the copolymer was verified by ^{1}H NMR. After 3 day dialysis (MWCO: 3500) against Ace:H_2O (80:20 v/v) mixture followed by lyophilization, the fatty acid-mimetic copolymers were further characterized by ^{1}H NMR (Figure S4) and GPC (Figure S5).

^{1}H NMR (DMSO-d_6, 400 MHz in ppm): 12.32 (1H, O═C-$\underline{OH}$), 3.87 (2H, -O-$\underline{CH_2}CH_2$-), 1.57 (2H, -O-$CH_2\underline{CH_2}$-), 1.28 (18H, CH_2-($\underline{CH_2}$)$_6$-CH_3), 0.91 (3H, -C-$\underline{CH_3}$), 0.80 (3H, -C-$\underline{CH_3}$)

Preparation and Characterization of Block Copolymer Micelles. P(PEGMA-*co*-PDSM)-*b*-(LMA-*co*-MAA) micelles were obtained by dissolving 10 mg of polymer in 200 μL of methanol:dimethyl sulfoxide (MeOH:DMSO; 80:20 v/v) followed by the slow addition of 0.1 M HEPES buffer (pH 7.4, Gibco) yielding a final concentration of 5 mg/mL. For in vivo studies, MeOH:DMSO was removed by buffer exchange into 0.1 M HEPES via 4 cycles of centrifugal dialysis (Amicon, MWCO 3000, Millipore). Prior to use, micelle solutions were filter sterilized (0.22 μm, Pall Corporation) and copolymer concentrations were determined via UV−vis spectroscopy (Synergy H1Multi-Mode Reader, BioTek). The critical micelle concentration (CMC), size, surface charge, and morphology of each

DOI: 10.1021/acsbiomaterials.6b00408
ACS Biomater. Sci. Eng. 2017, 3, 179−194

block copolymer were characterized through fluorescence spectroscopy (Synergy H1Multi-Mode Reader, BioTek), dynamic light scattering (DLS), ζ-potential, and transmission electron microscopy (TEM, FEI Tecnai Osiris), respectively. Polymer CMC values were determined using fluorescence and particle stability studies. Nile red (NR, Sigma-Aldrich), a hydrophobic dye that exhibits strong fluorescence within intact micelles,[50] was utilized as the fluorescence probe. Polymer solutions were prepared at varying concentrations from 0.0001 to 1 mg/mL and were incubated with NR stock solution (1 mg/mL in MeOH:DMSO (80:20)) at a 100:1 (v/v) ratio for 24 h under continuous stirring in the dark at RT. Samples were filtered (0.45 μm PTFE, Thermo Scientific) and the excitation spectrum of NR was measured in 96-well plates (UV-Star Microplates, Greiner Bio-One) at an excitation wavelength of 550 nm and the emission was monitored from 580 to 680 nm. The stability, hydrodynamic size, and ζ-potential of polymer micelles were analyzed by DLS using a Malvern Instruments Zetasizer Nano ZS Instrument (Malvern, USA) equipped with a 4 mV He−Ne laser operating at λ = 633 nm, an avalanche photodiode detector with high quantum efficiency, and an ALV/LSE-5003 multiple tau digital correlator electronics system. To determine the concentration at which the micelles exhibited morphological changes, particle sizes were measured over 10-fold range of serial dilutions with HEPES from 1 mg/mL to 0.001 mg/mL. TEM samples were prepared by placing 10 μL of micelle solution (1 mg/mL) onto copper grids (Formvar stabilized with carbon 400 mesh, Ted Pella Inc.). After 2 min of incubation, the excess solution was removed with filter paper and the grids were left to dry overnight before being imaged by TEM.

Drug Encapsulation Efficiency and Release Profile. A polymer micelle solution of 5 mg/mL was incubated with IMQ (Santa Cruz Biotechnology, Inc.) at a ratio of 3.3:1 (w/w) under continuous shaking (1100 rpm) for 48 h at RT. Nonencapsulated and insoluble IMQ was removed by centrifugation (4000g for 5 min) followed by sterile filtration (0.22 μm). IMQ concentration was quantified in solvent-resistant UV-Star microplates via diluting 10 μL of IMQ-loaded micelle solution in 90 μL of DMSO and measuring fluorescence at excitation/emission wavelengths of 325/365 nm. A calibration curve of fluorescence intensity vs IMQ concentration (ranging from 6.25 to 200 μM with an R^2 value of 0.99) prepared in a similar fashion (DMSO:HEPES 9:1, v/v) was used for calculating the amount of IMQ encapsulated in the micelles. Drug loading capacity (DLC) was determined through the ratio of encapsulated IMQ to total micelles (mg/g).[51]

To assess IMQ release kinetics, we placed 100 μL of IMQ loaded micelles were placed in a dialysis device (Slide-A-Lyzer MINI Dialysis Device, MWCO 3500, 0.5 mL, ThermoFisher Scientific) and dialyzed against 5 mL of buffer solutions (0.3 M sodium acetate (pH 5.0), 0.1 M phosphate buffer (pH 7.4) or phosphate-buffered saline (PBS) supplemented with 10% Heat Inactivated-Fetal Bovine Serum (HI-FBS, Gibco)) under continuous stirring. The buffer was collected and replaced with 5 mL of fresh buffer at predetermined time points. The collected dialysates were lyophilized, reconstituted in buffer-dependent solvent mixtures (DMSO:H_2O (1:1 v/v) for pH 5.0, DMSO:TFA:HCl (4:6:1 v/v) for pH 7.4 and DMSO:H_2O:HCl (2:4:1 v/v) for PBS supplemented with 10% FBS buffered samples) and the concentration of IMQ was determined via fluorescence spectroscopy using a calibration curve comprising standard solutions of IMQ in their respective solvent mixtures.

Assessment of In Vitro Cytotoxicity. Antigen presenting cells [bone marrow-derived dendritic cells (BMDC) and RAW264.7 (macrophages)] and tumor cells [B16−F10 murine melanoma cell line and A549 human lung adenocarcinoma epithelial cell line] were used to assess the toxicity of both empty and drug loaded micelle solutions at various concentrations. RAW264.7 and B16−F10 lines were grown in Dulbecco's Modified Eagle Medium w/L-Glutamine (DMEM, Gibco) containing 4.5 g/L glucose while A549 cells were cultivated in Kaighn's Modification of Ham's F-12 Medium (F-12K, ATCC) containing 1.5 g/L sodium bicarbonate; both growth mediums were supplemented with 10% HI-FBS. BM cells were isolated from both the femurs and tibias of 8−12 week old male wild-type C57BL/6J mice. After muscle tissue removal and ethanol sterilization of the bones, bone marrow was flushed out over a strainer with Dulbecco's phosphate-buffered saline (DPBS; Corning). Cells were then rinsed with DPBS, lysed using ACK Lysis buffer, (Gibco) and resuspended in complete growth medium GM-RPMI (Roswell Park Memorial Institute medium w/L-Glutamine (RPMI-1640, Gibco) supplemented with 10% FBS, 1% Penicillin Streptomycin (Gibco), 10 mM HEPES, 1X nonessential amino acids (Sigma-Aldrich), 1 mM sodium pyruvate (Gibco), 55 μM 2-mercaptoethanol (Sigma-Aldrich), 50 μg/mL Gentamycin (Life Technologies), 2.5 μg/mL Amphotericin B (Corning) and 10 ng/mL Granulocyte-macrophage colony-stimulating factor (GM-CSF, Peprotech)). BMDC emerging from this were cultured and supplemented with additional GM-RPMI on days 3 and 7 and were employed in experiments on days 8 to 12 after harvest.

BMDC, RAW264.7, B16-F10, and A549 were seeded into 96-well plates (appropriate number of cells needed for each well was determined from growth curves: 5×10^3 cells/well for B16−F10 and 10×10^3 cells/well for BMDC, RAW264.7, and A549) and incubated at 37 °C in 5% CO_2 and 95% humidity for 24 h to ensure adherence. Upon surface attachment, cells were incubated with both empty and IMQ-loaded micelles at varying concentrations (5−500 μg/mL). After 24 h of incubation, 20 μL of AlamarBlue dye was added to each well, and incubated for an additional 5 h.[52] Absorbance was measured at 570 nm and percent viability was expressed with respect to untreated cells (i.e., 100% viable). The treatments were done with four replicates and the assay was independently repeated three times.

In Vitro Evaluation of the TLR7 Pathway Activation in RAW-Blue Macrophages. RAW-Blue reporter cells (InvivoGen), a RAW264.7 macrophage derivative that contains an NF-κB and AP-1 inducible secreted embryonic alkaline phosphatase (SEAP) construct, were employed to investigate the effect of micellar IMQ delivery on TLR7 activation. Cells were seeded in 96-well plates at 15×10^4 cells/well concentration (180 μL/well) and incubated with empty micelles, free, and encapsulated-IMQ treatments (20 μL/well) at various concentrations for 24 h. Because of poor solubility in 0.1 M HEPES, free IMQ treatments were prepared from a stock solution in DMSO (1 mg/mL) which was then diluted into cell culture medium to desired concentrations. To measure SEAP levels, cell culture supernatants (50 μL/well) were incubated with 150 μL/well of the SEAP substrate QUANTI-Blue (InvivoGen) in a 96-well plate for 3 h at 37 °C. SEAP levels were determined by UV−vis measurements at 650 nm.

In Vitro BMDC Activation and Maturation. BMDCs were seeded at 2×10^5 cells/well (in 24-well plates) and 1×10^6 cells/well (in 6-well plates) 24 h prior to treatment. Cells were incubated with empty micelles, free, and encapsulated-IMQ treatments at various concentrations for 24 h. BMDCs treated with only 0.1 M HEPES and only lipopolysaccharide (LPS, 5 μg/mL, eBioscience) in RPMI medium were used as negative and positive controls, respectively. Cell supernatants in the 24-well plates were collected and analyzed for different cytokines (IL-6, TNFα, IL-1β, and IL-12) by ELISA (ELISA Ready-SET-Go! eBioscience) following the manufacturer's protocol. Cell surface immunostaining was employed for investigating BMDC maturation. Accordingly, cells cultivated in 6-well plates were harvested, preincubated with TruStain fcX (BioLegend) for 10 min on ice to block the Fc receptors, and subsequently stained with fluorescently labeled antibodies anti-CD40-PE, anti-CD80-APC, anti-CD86-PE-Cy7, and anti-MHC-II-APC-Cy7 (BioLegend) for 30 min at 4 °C. LPS stimulated BMDCs were stained with isotype controls (BioLegend) and used in background subtraction. Ten thousand events were acquired by LSRII flow cytometry (BD Biosciences) and the data was analyzed via FlowJo Software (Tree Star v10.0.8).

Preparation of Micelle-Antigen Conjugates. Polymer micelles were decorated with ovalbumin protein [OVA; Sigma-Aldrich (for in vitro studies) or EndoFit ovalbumin, InvivoGen (for in vivo studies)] via thiol−disulfide exchange. Following manufacturer's instructions, OVA was first labeled with either fluorescein isothiocyanate (FITC, Thermo Scientific) or AlexaFluor488-TFP (Invitrogen) with a degree labeling of ~1 dye/OVA. OVA was then thiolated using 25 molar excess of 2-iminothiolane (Traut's reagent, Thermo Scientific) and

DOI: 10.1021/acsbiomaterials.6b00408
ACS Biomater. Sci. Eng. 2017, 3, 179−194

buffer exchanged into 1X PBS using a Zeba desalting column (0.5 mL, MWCO 7000, Thermo Scientific) as previously described.[33] After sterile filtration (0.2 μm) the number of thiols per protein (4−5 thiols/OVA) were determined with Ellman's reagent (Thermo Scientific). Polymer micelle solutions were reacted with thiolated-OVA at various molar ratios in 0.1 M HEPES (pH 7.4) overnight in the dark at RT under continuous shaking. Antigen conjugation and subsequent disulfide reduction with 20 mM tris(2-carboxyethyl)-phosphine hydrochloride (TCEP, Sigma-Aldrich) was verified via gel electrophoresis using 4−20% Mini-Protean TGX Precast Protein Gel (Bio-Rad). The free micelle lanes (LMA50 and LMA50-IMQ) were used for subtracting background fluorescence from their respective conjugates (OVA-LMA50 and OVA-LMA50-IMQ). Gels were imaged (Gel Doc EZ, Bio-Rad) and conjugation was quantified with Image Lab (Bio-Rad) software.

In Vitro Antigen and IMQ Uptake by APCs. Intracellular uptake of vaccine formulations was evaluated in a dendritic cell line (DC2.4) using AlexaFluor488-labeled OVA (OVA488), a model fluorescent hydrophobic drug (NR), and IMQ. Cells were plated at 7.5×10^3 cells/well in 24-well plates and allowed to adhere overnight. DCs were then incubated with treatments groups containing 10 μg OVA488 with or without 2.5 μg IMQ and/or 0.12 mg polymer for 24 h. The formulations were as follows: free OVA488, OVA488 conjugated to polymer (OVA488-LMA50), IMQ encapsulated by polymer-OVA488 conjugates (OVA488-LMA50-IMQ), OVA488 mixed with IMQ (OVA488+IMQ), free NR, NR encapsulated by polymer-OVA488 conjugates (OVA488-LMA50-NR) and free OVA488 mixed with NR (OVA488+NR). To provide an accurate comparison among treatment groups, OVA controls used for in vitro uptake (OVA488) and MHC-I presentation (OVA) studies were thiolated proteins. Consistent with the encapsulation protocol used in CMC investigations, polymer solutions (5 mg/mL) were incubated with NR (1 mg/mL in MeOH:DMSO (80:20)) for 24 h at RT. Excess dye was removed by sterile filtration, the encapsulated dye content was quantified and matched to the dye content of all NR formulations. After 24 h, cells were collected, rinsed twice with PBS, and resuspended in flow cytometry staining (FACS) buffer (PBS containing 2% HI-FBS). Flow cytometry (Guava easyCyte, EMD Millipore) was used to monitor the uptake of OVA and NR.

In Vitro MHC-I Antigen Presentation. DC2.4 cells were employed as model antigen presenting cells to analyze the effect of IMQ and polymer carriers on MHC class I (MHC-I) presentation. DC2.4 (H-2K^b-positive) cells were kindly provided by K. Rock (University of Massachusetts Medical School) and cultured in RPMI supplemented with 10% HI-FBS, 2 mM L-glutamine, 1% Penicillin Streptomycin, 55 μM 2-mercaptoethanol, 1× nonessential amino acids, and 10 mM HEPES. This study utilized a 25-D1.16-PE monoclonal antibody (eBioscience) which recognizes the immunodominant $OVA_{257-264}$ epitope SIINFEKL bound to H-2K^b, a murine MHC-I molecule.[53] DC2.4 cells were seeded in 12-well plates at 2×10^5 cells/well and incubated for 24 h to ensure adherence. Cells were incubated with a variety of formulations (free OVA, OVA-LMA50, OVA-LMA50-IMQ, and OVA+IMQ) featuring 40 μg OVA with or without 10 μg IMQ and/or 0.5 mg polymer for 24 h. As a positive control, untreated cells were pulsed with 20 μM $OVA_{257-264}$ (InvivoGen) peptide for 2 h prior to staining. After incubation, cells were rinsed with PBS, detached, and resuspended in fresh FACS buffer. After TruStain fcX treatment, cells were stained with 25-D1.16-PE for 30 min at 4 °C, washed twice with FACS buffer, and analyzed via flow cytometry (Guava easyCyte, EMD Millipore).

Animals. Male C57BL/6 mice (6−8 weeks) were purchased from The Jackson Laboratory (Bar Harbor, ME), maintained at the animal facilities of Vanderbilt University under conventional conditions, and experimented upon in accordance with the regulations and guidelines of Vanderbilt University Institutional Animal Care and Use Committee (IACUC).

Intranasal Immunization. Low endotoxin grade OVA (<1 EU/mg, EndoFit) and sterile buffer solutions (1X PBS or 0.1 M HEPES at pH 7.4) were used for vaccine formulations. Endotoxin levels of the copolymer vaccines were tested using a ToxinSensor Chromogenic LAL endotoxin assay kit (GenScript) and found to be ≤5 EU/mL as recommended by the United States Pharmacopoeia.[54] The two experimental groups were IMQ encapsulated by polymer-OVA conjugates (OVA-LMA50-IMQ) and OVA mixed with soluble IMQ (OVA+IMQ). Formulations were prepared 3 days prior to immunization and were stored sterile at 4 °C. Polymer solutions buffer exchanged into 0.1 M HEPES were incubated with IMQ for 48 h. Following the removal of free IMQ via centrifugation and sterile filtration as described above, IMQ-loaded polymers were conjugated with freshly thiolated endotoxin free OVA (4 thiols/OVA in PBS) overnight. The control formulation, OVA+IMQ, was prepared by mixing OVA and soluble IMQ (5 mg/mL in 0.1 M lactic acid, Sigma-Aldrich) overnight.

Mice were anesthetized with ketamine/xylazine (10 mg/mL ketamine hydrochloride injection, Vedco; 1 mg/mL xylazine hydrochloride injection; Vanderbilt Pharmacy) by intraperitoneal (i.p.) injections (100 μL anesthesia/18 g mice). Groups of anesthetized mice ($n = 5$) were immunized intranasally (i.n.) on day 0 with formulations containing 40 μg OVA and 10 μg IMQ with or without 0.5 mg polymer. Vaccine formulations were delivered through the nostrils into the lungs at 100 μL/mouse. Animals were monitored every day from day 0 to day 12 for weight loss and signs of distress.

Analysis of OVA-Specific CD8$^+$ T cell Responses. On day 12 after immunizations, mice were anesthetized and administered 200 μL of anti-CD45-APC antibody (BD Biosciences) intravenously (i.v.). This procedure stains leukocytes in the vasculature. Five minutes after injection, mice were euthanized with CO_2, and broncheoalveolar lavage (BAL) fluid, lungs, and spleens were collected from each mouse. Organs were harvested and processed as previously described.[55] In brief, organs were passed through a 70 μm cell strainer and were lysed with ACK lysing buffer (Gibco) forming single cell suspensions. Prior to processing, lung samples were minced with a scalpel and incubated for 1 h at 37 °C in complete RPMI medium supplemented with 2 mg/mL collagenase (Sigma-Aldrich) and 50 nM dasatinib (LC Laboratories). Single cell suspensions from the BAL fluid, lungs, and spleens were stained at 4 °C with anti-B220-FITC (BD Biosciences), anti-CD4-FITC (BD Biosciences), anti-CD11b-FITC (Tonbo Biosciences), anti-CD11c-FITC (Tonbo Biosciences), anti-CD8α-PacificBlue (BD Biosciences), and 1.5 μg/mL of PE-labeled $OVA_{257-264}$ (SIINFEKL)-H-2K^b tetramer prepared according to a previously reported procedure.[56] After 1 h, cells were rinsed and stained with propidium iodide (BD Biosciences) to discriminate live from dead cells. LSRII flow cytometry (BD Biosciences) determined the frequency of OVA-specific CD8$^+$ T cells (tetramer-positive, CD8-positive population) and all data were analyzed using FlowJo Software (Tree Star v10.0.8).

Measurement of Antigen-Specific IgG Production in Sera of Immunized Mice. Retro-orbital blood draws were performed using plain capillary tubes (Fisher Scientific) 2 days prior to sacrifice (day 10), and serum was isolated and stored at −20 °C until further analysis. ELISA microtiter plates (Nunc MaxiSorp) were coated with 10 μg/mL OVA in 1X PBS and incubated overnight at 4 °C and blocked with PBS/0.01% Tween 20 (PBST; Sigma-Aldrich) for 1 h at RT. Starting from a 1:25 dilution, serum was added to the wells in 3-fold serial dilutions in PBST. In parallel, control-serum from naïve mice was used to determine the background. Following a 2 h incubation period, plates were rinsed with PBST (4X) and incubated with secondary antibody (goat antimouse IgG conjugated to horseradish peroxidase (HRP), Southern Biotech; diluted 1:5000) for 1 h at RT. After washes, antibody binding was detected with 100 μL of 1-step ultra TMB-ELISA substrate (ThermoFisher); after stopping HRP reaction with 2 N H_2SO_4 (Sigma-Aldrich), absorbance was measured at 450 nm, end point titers were determined from the reciprocal of serum dilution corresponding to 2.5× higher absorbance value than that of the control-serum.[30]

Statistical Analysis. Data analysis was performed on Graphpad Prism software using one-way analysis of variance (ANOVA) coupled with Tukey's post-test to compare statistical significance among multiple groups (>2). Differences between two groups were analyzed by an unpaired, t test. Results were expressed as the mean of a minimal

DOI: 10.1021/acsbiomaterials.6b00408
ACS Biomater. Sci. Eng. 2017, 3, 179−194

Table 1. Properties of Copolymers for Dual Delivery of Protein Antigen and IMQ

$[M]_t$[a]	polymer composition	conversion[b] (%)	M_n[c] (g/mol)	$M_{n,theo}$[d] (g/mol)	$\Sigma M_{n,theo}$[e] (g/mol)	PDI[f]
		1st Block (P(PEGMA-*co*-PDSM))				
0.5	92 mol % PEGMA	36	13 700	11 000		1.09
		2nd Block Addition (P(PEGMA-*co*-PDSM)-*b*-(LMA-*co*-MAA))				
2	75 mol % LMA	74	25 000	16 700	27 700	1.01
2	50 mol % LMA	73	30 000	15 000	26 000	1.16
2	25 mol % LMA	71	28 000	12 000	23 000	1.06

[a]Total monomer feed concentration, polymerization conditions: solvent toluene and temperature 70 °C. [b]Monomer conversion determined by ^{1}H NMR. [c]The number of average molecular weight determined by GPC analysis. [d]The theoretical molecular weight calculated by $M_{n,theo}$= (([M]$_0$/[RAFT]$_0$)·conversion·MW$_{monomer}$) + MW$_{RAFT}$), where [M]$_0$, [RAFT]$_0$, conversion, MW$_{monomer}$, and MW$_{RAFT}$ are the initial monomer, and RAFT agent concentrations, monomer conversion, molecular weight of the monomer, and molecular weight of the RAFT agent, respectively. [e]The total theoretical molecular weight determined by the sum of the 1st and 2nd blocks. [f]Polydispersity index.

of two independent experiments ± SD, with ****P < 0.0001, ***P < 0.001, **P < 0.01, *P < 0.05 being considered statistically significant.

RESULTS AND DISCUSSION

Synthesis and Characterization of Fatty Acid-Mimetic Polymers. IMQ has demonstrated a promising solubility profile in the presence of long-chain fatty acids such as oleic acid (20 mg/mL) and isostearic acid (17 mg/mL),[21] which act as the primary solubilizing agents for the FDA-approved topical IMQ cream Aldara. Notably, solubility is dependent on both lipid and carboxylic acid groups as solubility in isopropyl palmitate and sorbitan monooleate is very low (<0.1 mg/mL).[21] Hence, we hypothesized that polymer micelles with a core comprising long alkyl chained hydrophobic groups and acidic moieties would facilitate encapsulation of IMQ.

To test this hypothesis, we synthesized a series of novel diblock copolymers with a hydrophilic first block of PEGMA and thiol-reactive PDSM groups, and a second block comprising variable compositions of a 12 carbon alkyl monomer (LMA) and an acidic monomer (MAA). Using the RAFT polymerization technique, which has been widely utilized for generating well-defined polymers with complex architectures, controlled molecular weights, and narrow molecular weight distributions,[47] P(PEGMA-*co*-PDSM)-*b*-(LMA-*co*-MAA) block copolymers were synthesized in a three-step process (Scheme S2).

To enhance stability and biocompatibility, we polymerized a hydrophilic first block composed of PEGMA and PDSM in the presence of CPABD, a dithioester RAFT agent that has been widely used for the polymerization of methacrylates.[57] PEGMA forms a brushlike conformation that has been shown to improve circulation times of macromolecules[58,59] while also enabling copolymerization with reactive monomers, such as PDSM.[59] The theoretical molecular weight (M_n) was calculated to be 11000 g/mol from ^{1}H NMR, whereas GPC analysis resulted in an experimental M_n of 13700 g/mol with a PDI of 1.09 (Table 1). The final composition of the first block consisted of 92 mol % PEGMA along with 8 mol % PDSM, which has been found to be a sufficient amount of pyridyl disulfide moieties for antigen conjugation by other nanocarriers that have been used for in vivo applications.[43,45,60]

Using P(PEGMA-*co*-PDSM) as a macro-RAFT agent, a second block was polymerized with LMA -a lipid-like monomer that serves the dual purpose of increasing IMQ solubility and driving micelle formation- and *t*-BMA monomers. Because of the difference in solubility and rate of polymerization among MAA and LMA monomers,[57] *t*-BMA was initially copolymerized with LMA then acid hydrolyzed forming MAA units. *Tert*-butyl esters are effective protecting groups on account of their acid-cleavable labile ester-alkyl bonds.[61−63] Studies have shown a strong correlation between the size of a micelle's hydrophobic core and its DLC,[64] with a hydrophobic to hydrophilic block ratio of 1.5 demonstrating augmented drug loading properties;[65] thus fatty acid-mimetic copolymers were designed with the same core to corona ratio.

To obtain polymers of varying hydrophobic and acidic composition, we performed polymerizations with increasing LMA content in the feed (Table 1). The composition of the second block was calculated from the integrations of relevant LMA and *t*-BMA proton signals in the ^{1}H NMR spectra at 3.93 ppm (2H) and 1.41 ppm (9H), respectively (Figure S3). The final polymer composition reflected the monomer mole ratio in the feed, indicating statistical placement of the two monomers along the second block of the polymer chain. Following chain extension, copolymer peaks shift to higher molecular weights and display a monomodal GPC trace, indicating that the polymerization occurs in the absence of side reactions that can trigger branched or terminated polydisperse chains (Figure S5).

Conversion of *tert*-butyl ester groups to carboxylic acids was achieved through a well-established selective TFA hydrolysis process that specifically cleaves *tert*-butyl moieties without affecting other types of esters.[66] Deprotection was monitored by ^{1}H NMR in DMSO-d_6 where the disappearance of the *tert*-butyl resonance at 1.41 ppm along with the formation of an acidic proton at 12.32 ppm confirmed the completion of hydrolysis (Figure S4). A clear increase in polymer solubility in polar organic solvents (e.g., DMF) was another indicator of ester bond cleavage. To verify the selective deprotection of *tert*-butyl groups with TFA, a control experiment was conducted where the macroRAFT and P(PEGMA-*co*-PDSM)-*b*-(LMA) (LMA100; $M_{n,theo}$ = 31 000 g/mol) polymers were separately treated with TFA for 30 h at RT. Results indicated that acid hydrolysis conditions applied for the cleavage of *tert*-butyl ester did not cleave ester linkages within the other monomers.

Diblock Copolymers Self-Assemble into Micellar Nanoparticles with a Fatty Acid-Mimetic Core. To generate nanoparticles with a fatty acid-mimetic core for the encapsulation of IMQ, polymer micelles were formed by the self-assembly of P(PEGMA-*co*-PDSM)-*b*-(LMA-*co*-MAA) chains in aqueous solution (Figure 1A, B). Solubility trials were conducted using a range of water-miscible, organic cosolvents, and a mixture of MeOH:DMSO (80:20 v/v) was ultimately found to solubilize all polymers in the series with varying oleophilic content (i.e., LMA25, LMA50, and LMA75). Micelles were prepared by dissolving the copolymers in the organic cosolvent at 50 mg/mL followed by diluting the

DOI: 10.1021/acsbiomaterials.6b00408
ACS Biomater. Sci. Eng. 2017, 3, 179−194

Table 2. Characteristics of Block Copolymer Micelles for IMQ Delivery

	size[b] (nm)		PDI[b]		IMQ loading[c] (μg/mL)			
block copolymer[a]	empty	IMQ loaded	empty	IMQ loaded	24 h	48 h	w/w[d] (%)	CMC[e] (mg/mL)
LMA100	346 ± 2.2	346 ± 2.9	0.25	0.21	9.8 ± 0.5	7.8 ± 1.9	0.16	0.081
LMA75	51.6 ± 0.4	88.3 ± 0.7	0.08	0.25	23.5 ± 1.5	25.4 ± 1.4	0.51	0.093
LMA50	30.1 ± 0.1	36.2 ± 0.3	0.14	0.29	82.2 ± 1.9	111.6 ± 4.8	2.23	0.088
LMA25	21.4 ± 0.1	27.2 ± 2.9	0.47	0.57	80.2 ± 2.7	91.9 ± 4.2	1.84	0.165
LMA0	21.3 ± 0.2	15.1 ± 0.1	0.75	0.56	22.8 ± 0.2	26.6 ± 2.0	0.53	n/a

[a]Control block copolymers: (PEGMA-*co*-PDSM)-*b*-(LMA) ($M_{n,theo}$ = 31 000 g/mol) and (PEGMA)-*b*-(MAA) ($M_{n,theo}$ = 30 000 g/mol) are represented as LMA100 and LMA0, respectively. [b]Determined by means of DLS for micellization in 0.1 M HEPES. [c]IMQ loading calculated after 24 and 48 h of polymer:IMQ (3.3:1, w/w) encapsulation at RT (n = 3). [d]The average weight/weight (%) loading for 48 h is calculated by w/w% = amount of encapsulated IMQ/amount of polymer x 100. [e]CMC values of block copolymers determined by using a fluorescent probe, i.e., NR (n = 2).

solutions 10-fold into HEPES buffer (pH 7.4). The gradual dilution process allowed the polymers to spontaneously self-assemble into micelles with P(PEGMA-*co*-PDSM) forming an outer shell around the P(LMA-*co*-MAA) core. The size, surface charge, and morphology of LMA75, LMA50, and LMA25 copolymers was characterized in comparison to *control*-block copolymers, LMA100 and LMA0 ((PEGMA)-*b*-(MAA); $M_{n,theo}$ = 30 000 g/mol), which were synthesized to represent both ends of the copolymer composition spectrum.

DLS measurements indicated average hydrodynamic diameters of 51.6, 30.1, and 21.4 nm for LMA75, LMA50, and LMA25 respectively (Figure 1C and Figure S6A, B). The hydrodynamic diameter of micelles (Table 2) displays a strong correlation between increased LMA content and the micelle size, a likely result of the sterically demanding LMA units within the core increasing chain persistence length and occupying a higher volume.[65,67] TEM imaging (Figure S6C) of LMA50 confirmed particle size and indicated a spherical particle morphology. Also consistent with micellar assembly, the negative charges originating from MAA moieties were successfully shielded by the PEGMA corona in LMA75 and LMA50 copolymers, resulting in ζ-potential measurements of 0.025 and 0.018 mV, respectively. A decrease in the ζ-potential is observed for LMA25 (−8.45 mV) because of the higher mole ratio of MAA and lower feed molar ratio of steric LMA groups, which are proficient at hindering charge,[68] within the copolymer structure.

Two complementary methods, a fluorescence probe technique and DLS stability assay, were used to determine the critical micelle concentration (CMC) of micelles of variable core LMA content.[69,70] The fluorescence intensity of NR, a well-established lipophilic florescent probe,[71,72] was measured as a function of polymer concentration. At concentrations above the CMC, NR exhibits dramatically higher fluorescence emission, indicating that the dye is encapsulated in a hydrophobic micellar core (Figure S7A, B). The CMC values of LMA75, LMA50, and LMA25 copolymers were estimated to be 0.093, 0.088, and 0.165 mg/mL, respectively, which is similar to other block copolymer micelles used for hydrophobic drug delivery reported in the literature (Table 1).[51,73,74] To validate CMC measurements, we used a DLS-based dilution method in which hydrodynamic diameters of copolymers were measured at concentrations ranging from 1 mg/mL to 0.001 mg/mL (Figure S7C and Table S1). Particle size remained stable between 0.1−0.01 mg/mL (for LMA75 and LMA50) and 0.5−0.1 mg/mL (for LMA25), consistent with the CMC range determined with NR encapsulation.

Compared to the other copolymers, LMA25 demonstrated a nearly 2-fold increase in its CMC value as result of its higher negative charge and reduced core hydrophobicity. As expected, LMA0 was not able to form micelles, likely existing as unimers in aqueous solution due to the absence of hydrophobic micellar driving forces in the second block. The small size, neutral zeta potential, and brushlike PEGMA shell render fatty acid-mimetic carriers well-suited for increasing drug circulation time, enhancing lymphatic drainage from injection sites,[39] and facilitating passive accumulation at tumor sites via the enhanced permeation and retention (EPR) effect.[40,75] Though micelles were specifically designed to accommodate the unique solubility requirements of IMQ, they also have potential utility as carriers for hydrophobic drugs or cationic macromolecules.

IMQ Encapsulation and Release from Fatty Acid-Mimetic Micelles. Based on the high solubility of IMQ in fatty acids, but not other organic solvents, we postulated that a micelle core comprising a statistical copolymer of long alkyl chain and carboxylic acid monomers would provide a favorable environment for IMQ loading. To evaluate this and to elucidate how the molar ratio of alkyl chains to acidic groups influences IMQ solubility, the DLC of IMQ in each micelle formulation was quantified. Preformed micelles were incubated with IMQ for 24 and 48 h under continuous stirring. Under the same conditions, a control sample without micelles was prepared to determine IMQ solubility in 0.1 M HEPES (4.5 and 6.0 μg/mL for 24 and 48 h, respectively). As additional controls, structurally analogous diblock copolymers lacking acidic groups (LMA100) or without a micellar morphology (LMA0) were prepared. Free IMQ was removed by centrifugation and filtration, followed by a 10-fold dilution into DMSO, facilitating the release of IMQ which was then quantified via fluorescence spectroscopy. In order to determine the maximum DLC, the weight ratio of polymer to IMQ was varied between 10:1−1.25:1 at a constant polymer concentration, resulting in a plateau (maximum DLC) at 3.3:1 ratio (Figure S8), which was used for all subsequent encapsulation studies.

The loading efficiency of LMA100 micelles was largely negligible (0.16 w/w%), with a similar solubility to IMQ in HEPES buffer, whereas LMA0 increased solubility nearly 3.5-fold, likely due to IMQ's preference for acidic groups and ability to form hydrogen bonds with MAA.[76] These results demonstrate the importance of acidic groups for solubilization of IMQ and motivate the design of micelles comprising both LMA and MAA in the core. Indeed, the loading efficiencies of LMA75, LMA50, and LMA25 were revealed to be 0.51, 2.23, and 1.84 w/w%, respectively (Table 2). The hydrodynamic diameter of the loaded micelles revealed a slight increase in size

DOI: 10.1021/acsbiomaterials.6b00408
ACS Biomater. Sci. Eng. 2017, 3, 179−194

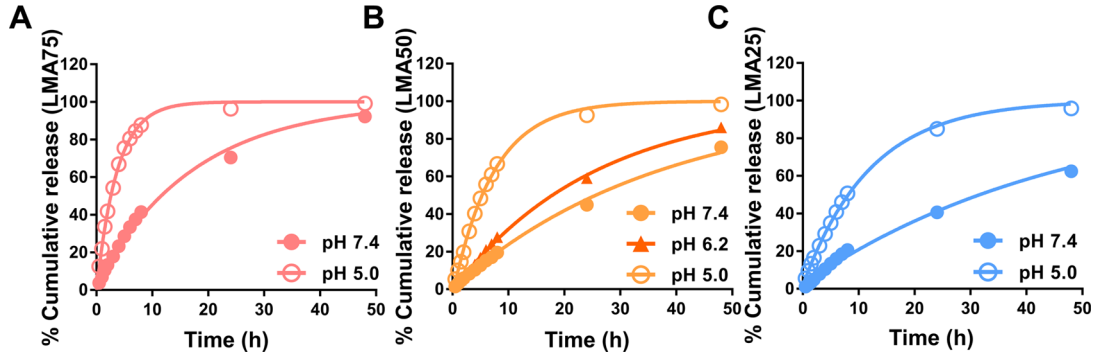

Figure 2. Core composition of fatty acid-mimetic micelles influences the release kinetics of IMQ at physiological and early and late endosomal pH values. IMQ was encapsulated in (A) LMA75, (B) LMA50, and (C) LMA25 polymer micelles, dialyzed against buffers at pH 7.4, 6.2, and 5.0 and cumulative release was quantified over 48 h. 50% IMQ release values were determined by using exponential one-phase decay nonlinear fit analysis with R^2 values greater than 0.98. The 50% release time points for LMA75, LMA50, and LMA25 polymer micelles were revealed to be 12.1 ± 0.6, 25.7 ± 0.3, 32.7 ± 0.4 h (at pH 7.4) and 2.6 ± 0.7, 5.1 ± 0.6, 8.4 ± 0.4 h (at pH 5.0), respectively. Graphs represent the means and standard deviation from four individual experiments.

(Table 2) as a result of chain expansion in the hydrophobic core upon encapsulation. As expected, LMA75, the copolymer with the least acidic content, demonstrated the lowest loading of the three P(PEGMA-*co*-PDSM)-*b*-(LMA-*co*-MAA) block copolymer micelles, though comparable to the nonmicellar LMA0 formulation, suggesting an interplay between IMQ's interaction with acidic moieties and a hydrophobic environment. Interestingly, the highest IMQ loading was obtained with LMA50, consistent with mimicking the 1:1 molar ratio of alkyl chains to acidic groups characteristic of fatty acids. Notably, on a per mass basis, IMQ solubility in LMA50 micelles (2.2 w/w %) is comparable to reported solubility in isostearic acid (1.9 w/w%)[21] and approved topical formulations of Aldara (3.75 and 5 w/w%).[20]

The protonation of aromatic amines in IMQ under acidic conditions led us to postulate that the reduced pH encountered within tumor microenvironments or endo/lysosomes would enhance the release of encapsulated IMQ.[77] Specifically, IMQ binds TLR7 localized within acidic endosomal vesicles, and, therefore, must be released from micelles in response to decreases in pH.[29,78] To explore this, the release of IMQ encapsulated in micelles of varying LMA composition was assessed via dialysis against buffer solutions mimicking the cytosolic (pH 7.4) and late endosomal (pH 5.0) environments (Figure 2). At pH 7.4, 50% of IMQ was released from LMA75, LMA50, and LMA25 micelles after 12.1 ± 0.6, 25.7 ± 0.3, and 32.7 ± 0.4 h, respectively. Consistent with the interactions between IMQ and MAA, the copolymer with the lowest acidic content, LMA75, demonstrated the fastest drug release profile, and increasing the acidic character of the micelle core increased the retention time of IMQ by 2- and 3- fold for LMA50 and LMA25, respectively. Slightly faster release was observed with micelles in the presence of serum proteins (Figure S9). The 50% release time points for LMA75, LMA50, and LMA25 polymer micelles were revealed to be 4.6 ± 2.1, 16.2 ± 1.6, and 22.1 ± 1.1 h in PBS buffer supplemented with 10% FBS, respectively. This may reflect a destabilizing effect of serum proteins on the micelle core and reduced the retention time of the drug within the micelle, resulting in 1.5 to 2.5 times faster release at similar pH. At pH 5.0, the release kinetics of IMQ was significantly increased, displaying a burst-like effect due to IMQ's high solubility under acidic conditions with 50% IMQ released at 2.6 ± 0.7, 5.1 ± 0.6, and 8.4 ± 0.4 h time points for LMA75, LMA50, and LMA25, respectively. As a further demonstration of pH-responsive release kinetics, IMQ release from LMA50 was studied at the early endosomal pH of 6.2. As expected, the release profile laid between pH 5.0 and pH 7.4, exhibiting 50% drug release at 17.7 ± 0.2 h. We note that relative to a recently described polylactide-based IMQ delivery system, to our knowledge the only previously described micellar delivery system, fatty acid-mimetic micelles enable more stable IMQ encapsulation at physiological pH (i.e., 50% release at >10 h vs 1 h) and a more dramatic pH-triggered release profile.[74] Therefore, by rationally designing block copolymer micelles with an optimized fatty acid-mimetic core, we have developed a novel water-soluble, nanoparticle-based IMQ formulation with a smaller size and higher encapsulation efficiency than other sub-100 nm IMQ delivery vehicles reported to date.[74,78,79]

Fatty Acid-Mimetic Micelles are Highly Cytocompatible. Micelles were designed with a PEGMA-rich corona to impart high colloidal stability and minimal cytotoxicity. Prior to studying the immunomodulatory properties of IMQ-loaded micelles, the cytotoxicity of empty and IMQ-loaded micelles was investigated in antigen presenting cells (RAW264.7 and BMDCs) and cancer cell lines (B16−F10 and A549), owing to the exploration of IMQ as both a vaccine adjuvant and a cancer immunotherapeutic. Cells were treated with empty micelles at varying concentrations (5−500 μg/mL) for 24 h to determine the cytocompatibility of the carriers in vitro. Consistent with the neutral/anionic nature of the copolymers, no significant toxicity was observed in any of the cells tested (Figure 1D and Figure S10).

Subsequently, polymer carriers were loaded with IMQ (0.2, 1, 2, and 10 μg/mL drug encapsulated in 10, 50, 100, and 500 μg/mL micelle solutions, respectively) and cytotoxicity evaluated in the cells described above (Figure S11). Consistent with the empty micelles, IMQ-loaded particles displayed no cytotoxicity in the cells tested, though a dose-dependent increase in cell viability was observed for BMDCs (Figure S11B). This likely reflects IMQ's ability to increase BMDC proliferation and improve DC survival, which has been leveraged to enhance the efficacy of DC-based therapies.[32,80] The high cytocompatibility of fatty acid-mimetic micelles bodes favorably for in vivo applications, potentially enabling IMQ delivery via multiple routes.

Micellar Delivery Enhances IMQ Activity. To exert its immunomodulatory effects, IMQ must be delivered to

DOI: 10.1021/acsbiomaterials.6b00408
ACS Biomater. Sci. Eng. 2017, 3, 179−194

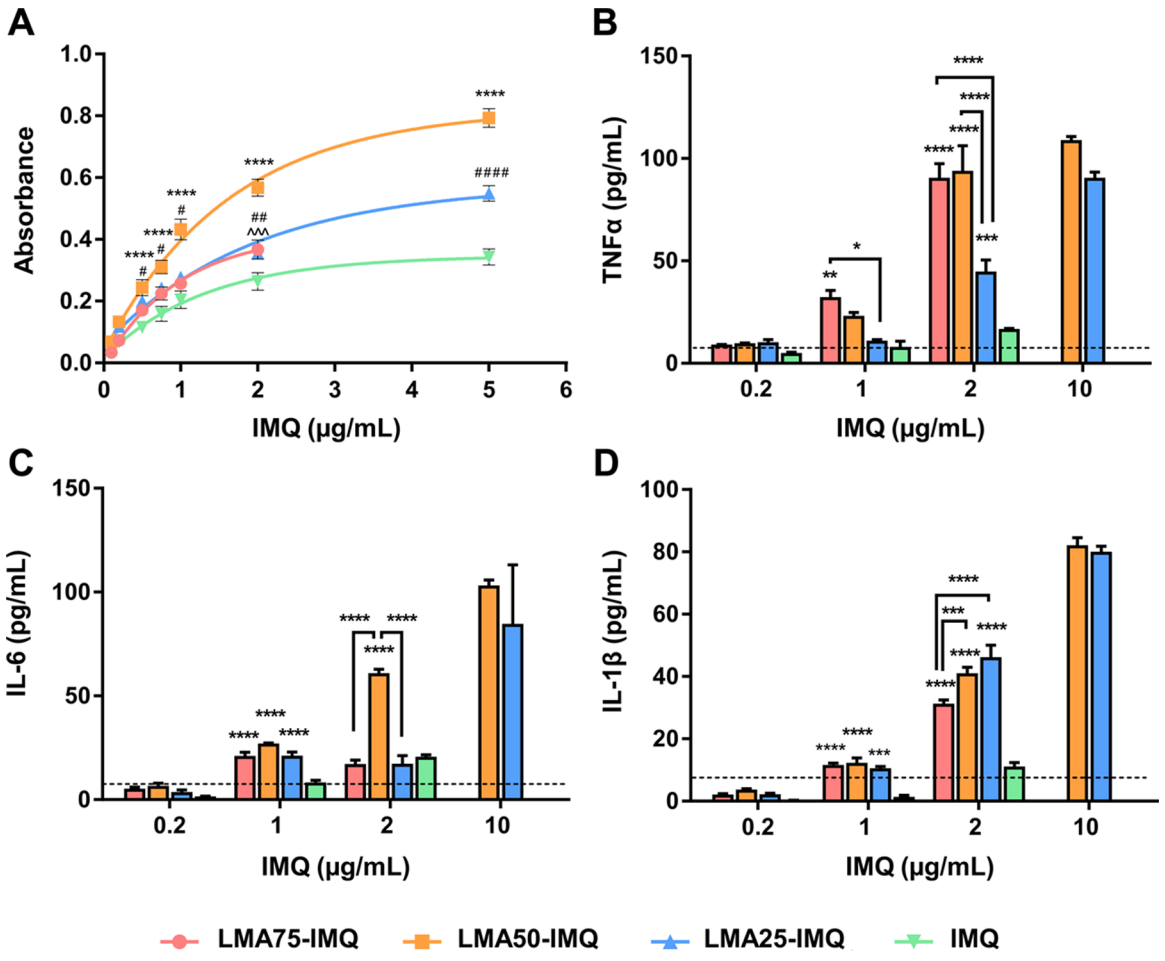

Figure 3. Micellar IMQ delivery enhances NF-κB activity resulting in increased cytokine production. (A) In vitro evaluation of NF-κB activation in RAW-Blue cells stimulated with 0.1−5 μg/mL free and encapsulated IMQ for 24 h. Statistical differences were observed between the loaded polymer micelles and soluble IMQ at higher doses and are represented as (#) LMA75-IMQ vs IMQ; (*) LMA50-IMQ vs IMQ; and (^) LMA25-IMQ vs IMQ. BMDCs were stimulated for 24 h with free and encapsulated IMQ at varying doses (0.2, 1, and 2 μg/mL). A higher IMQ dose, 10 μg/mL, was included in the studies with LMA50-IMQ and LMA25-IMQ being the only two formulations able to achieve this dose. Levels of proinflammatory cytokines (B) TNFα, (C) IL-6, and (D) IL-1β were measured by ELISA. The lower detection limit of each cytokine is represented by a dotted line. Statistical analysis revealed no significant difference between treatment groups at 0.2 and 10 μg/mL for all cytokines. Statistical analysis illustrated by (*) represents significance for each loaded micelle vs free IMQ, whereas significance among polymer micelles is indicated with tracing lines.

endosomal vesicles where TLR7 is stationed. Based on the propensity of macrophages and DCs to endocytose nanoparticles and the rapid pH-responsive release of IMQ from fatty acid-mimetic micelles (Figure 1B), we postulated that micellar delivery of IMQ would enhance immunostimulatory activity. Binding of IMQ to TLR7 stimulates innate immunity through the adapter molecule MyD88, resulting in the activation of the transcription factor NF-κB and the production of proinflammatory cytokines.[16] RAW-Blue cells that report on NF-κB induction via production of SEAP were utilized to evaluate the immunostimulatory activity of free and encapsulated-IMQ formulations. Free and encapsulated-IMQ treatments varied from 0.1 to 5 μg/mL, while empty micelle concentrations were equivalent to their IMQ-loaded counterparts. Both free and encapsulated-IMQ formulations stimulated NF-κB -dependent SEAP in a dose-dependent manner (Figure 3A), with all encapsulated formulations demonstrating increased activity over free IMQ at concentrations above 1 μg/mL. Empty micelles did not trigger NF-κB (Figure S12A), supporting the noninflammatory nature of the carriers and confirming IMQ-dependent NF-κB activation. Delivery of IMQ with LMA50 resulted in the most significant enhancement of activity, with a ∼3.5-fold increase of SEAP levels at concentrations >1 μg/mL. Although micelle-mediated enhancements in IMQ activity are likely in part due to increased bioavailability because of enhanced aqueous solubility, differences observed between carriers suggest a relationship between core composition and IMQ delivery. For example, the superior activity of LMA50 relative to LMA25 and LMA75 may reflect a requirement for balance between micelle stability, high drug loading, and rapid endosomal release. Elucidating the mechanisms by which fatty acid-mimetic micelles enhance IMQ activity will require further investigation. Nonetheless, to our knowledge this represents the first investigation into how material properties can be tuned to optimize IMQ solubility and activity.

Micellar IMQ Delivery Increases Dendritic Cell Activation and Maturation. Activation of TLR7 signaling induces DC maturation and stimulates the expression of proinflammatory cytokines, motivating exploration of IMQ as a vaccine adjuvant, cancer immunotherapeutic, and antiviral agent.[16,81] Hence, BMDCs were incubated with empty micelles, free, and encapsulated-IMQ treatments over a range of IMQ

DOI: 10.1021/acsbiomaterials.6b00408
ACS Biomater. Sci. Eng. 2017, 3, 179−194

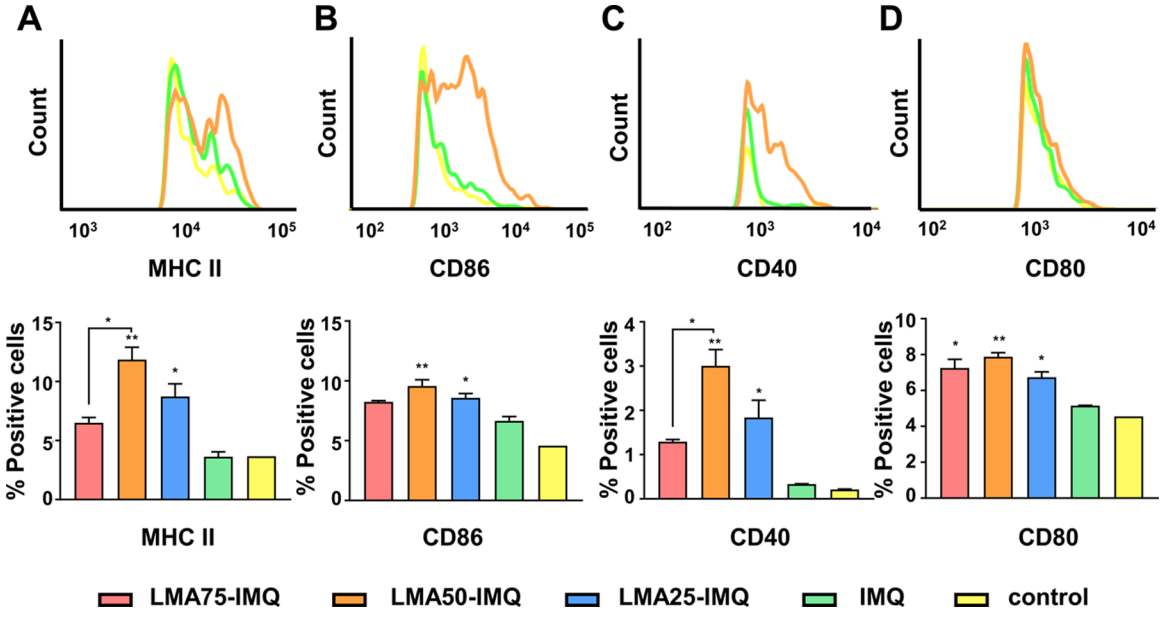

Figure 4. Micellar IMQ delivery enhances TLR7-driven BMDC activation and maturation. Flow cytometry was used to measure surface expression of BMDC maturation markers (A) MHC-II, (B) CD86, (C) CD40, and (D) CD80 induced by free and encapsulated IMQ. BMDCs were treated with 2 μg/mL IMQ for 24 h and were evaluated for their relative marker surface expressions (top) and percentage of marker positive cells (bottom). Representative histograms of untreated (control), IMQ, and LMA50-IMQ are shown for each marker. (*) represents the significant difference between micellar-IMQ vs free IMQ, whereas connected lines illustrate significance among different polymer micelles.

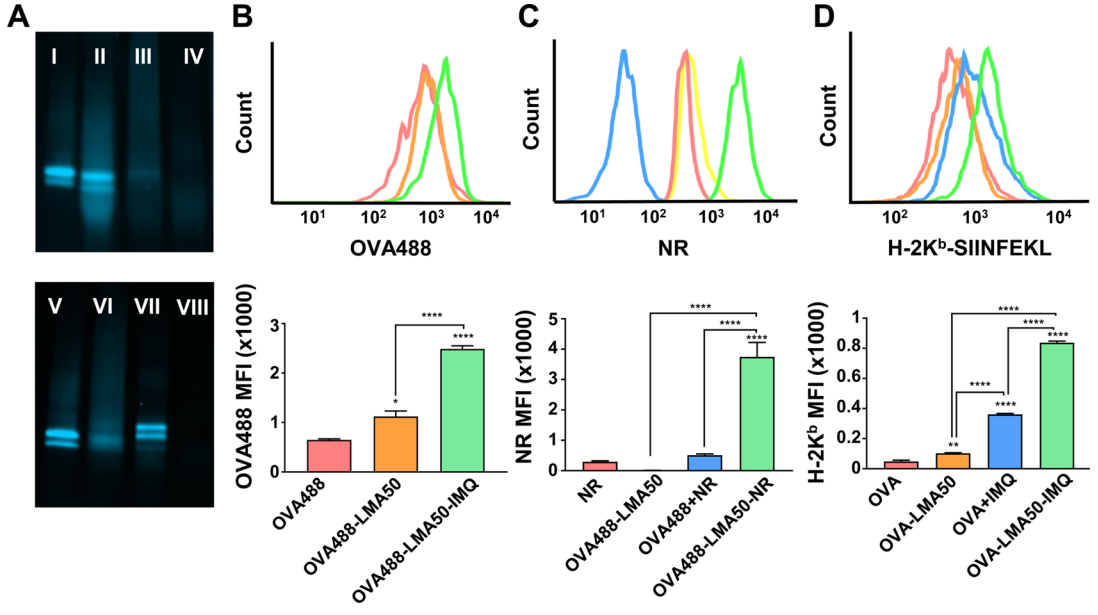

Figure 5. Conjugation of OVA to PDSM groups on micelle coronas enables coloading of antigen and IMQ, resulting in enhanced intracellular uptake and antigen cross-presentation. (A) FITC-labeled OVA was thiolated (4−5 thiols/OVA) (represented as I in the top gel and V in the bottom gel) and reacted with empty (III: OVA-LMA50) or IMQ-loaded micelles (VI: OVA-LMA50-IMQ) at 1:20 (OVA:polymer) ratio and SDS-PAGE was used to assess antigen conjugation and release of OVA upon incubation with TCEP (VII: OVA-LMA50-IMQ + TCEP). A physical mixture of nonthiolated OVA and LMA50 (II: OVA+LMA50) as well as formulations lacking OVA (IV: LMA50 and VIII: LMA50-IMQ) were run as controls. Flow cytometry was used to assess the effect of micellar delivery on the uptake of OVA488 and a model hydrophobic, fluorescent drug, NR by DC2.4 cells after 24 h incubation at 37 °C. (B) Uptake of OVA488: Representative histograms (top) and MFI values (bottom) of DC2.4 cells incubated with OVA488 (red), OVA488-LMA50 (orange), and dual delivery carriers (OVA488-LMA50-IMQ; green) treatment groups for 24 h. (C) Uptake of NR: DC2.4s treated with NR (red), OVA488-LMA50 (orange), a physical mixture of OVA488 and NR (OVA488+NR) (blue), and dual delivery carriers (OVA488-LMA50-NR; green) are illustrated in representative histograms (top) and MFI graphs (bottom). (D) The effect of IMQ and/or micellar delivery on MHC-I presentation by DC2.4 cells was assessed via flow cytometry using an antibody that recognizes MHC-I (H-2K^b)-bound SIINFEKL. Antigen cross-presentation is illustrated by representative histograms (top) and MFI graphs (bottom) of DC2.4 cells incubated with OVA (red), OVA-LMA50 (orange), OVA+IMQ (blue), and dual delivery carriers (OVA-LMA50-IMQ; green) for 24 h. Statistical analysis illustrated by (*) represents significance for each ova conjugated-loaded micelle vs control (free antigen or dye) and significance between different groups are shown with connected lines.

DOI: 10.1021/acsbiomaterials.6b00408
ACS Biomater. Sci. Eng. 2017, 3, 179−194

concentrations (0.2, 1, 2, and 10 μg/mL) and secreted TLR7-driven cytokines TNFα, IL-6, IL-1β, and IL-12p70 that were monitored. Overall, micellar formulations tended to enhance cytokine levels over free IMQ, although some compositional dependence was observed (Figure 3B-D). All formulations increased IL-1β production at 1 and 2 μg/mL compared to free IMQ 9- and 3-fold, respectively. Micellar IMQ encapsulation also enhanced TNFα production at 2 μg/mL, with LMA75 and LMA50 carriers mediating 2-fold higher TNFα production over LMA25 and 5 times greater than free IMQ. IL-6 expression was most strongly enhanced by a 3-fold increase in IL-6 production at both 1 and 2 μg/mL LMA50-IMQ over free IMQ. Likewise, LMA50-IMQ enhanced production of IL-12p70, at 2 μg/mL, although the levels were low and near the lower detection limit of the assay (Figure S13). Additionally, the high loading efficiency of LMA50 and LMA25 micelles enabled dosing at 10 μg/mL IMQ concentrations that was beyond its solubility limit, resulting in further enhancement of cytokine production. Consistent with NF-κB studies, empty micelles (without IMQ) corresponding to the same concentrations (10, 50, 100, and 500 μg/mL) did not elicit detectable cytokine production (Figure S12B–D).

The effect of micellar IMQ delivery on BMDC maturation was assessed via flow cytometric detection of the maturation markers CD80, CD86, CD40, and MHC-II (Figure 4). Treatment with IMQ-loaded micelles increased the frequency of marker-specific BMDCs with LMA50-IMQ and LMA25-IMQ mediating the most significant enhancements compared to free IMQ. Similarly, delivery with LMA50 and LMA25 increased expression levels (as determined by MFI of marker positive cells) of the costimulatory molecules CD40 and CD86 relative to free IMQ (Figure S14). In accord with BMDC activation studies, empty micelles (without IMQ) had no effect on BMDC maturation (Figure S15), verifying that the enhanced immunostimulatory effects result from the combination of fatty acid-mimetic micelles and IMQ. Collectively, these results demonstrate that fatty acid-mimetic micelles facilitate the delivery of IMQ in a highly water-soluble formulation with increased immunostimulatory activity, and, hence, have the potential to enhance the efficacy and expand utility of IMQ for in vivo applications. LMA50 micelles, which facilitated the highest IMQ loading, were particularly effective at enhancing TLR7 signaling, proinflammatory cytokine production, and DC maturation. Therefore, LMA50 was selected as the lead candidate for a novel subunit vaccine formulation based on nanoparticle-mediated codelivery of encapsulated IMQ and covalently conjugated protein antigen.

Fatty Acid-Mimetic Micelles Enable Dual Delivery of Antigen and IMQ. A number of studies have demonstrated improved T cell and antibody responses with subunit vaccines that codeliver protein antigens and TLR7 agonists with the same carrier.[18,30,36,37] To exploit this phenomenon, we designed micelles with a hydrophilic first block comprising PEGMA and thiol-reactive PDSM groups for the conjugation of thiolated-protein antigens. The reversible disulfide allows for liberation of antigens upon negotiating the reducing environment of the endosome or cytosol, resulting in improved antigen processing and enhanced immunogenicity.[45] Hence, the model protein antigen OVA was fluorescently tagged, thiolated, and reacted with LMA50 micelles. SDS-PAGE was used to evaluate antigen conjugation efficiency by monitoring the band shift and disappearance of FITC-labeled OVA (Figure 5A).[33,43,44] Using lane densitometry, approximately 88% conjugation was attained at a 1:20 molar ratio of protein:polymer (OVA:LMA50). As anticipated, coupling was not observed with the physical mixture of native OVA and polymer (OVA+LMA50 1:20 ratio) because of the lack of free cysteine residues in the protein.[33,82] Antigen conjugation to IMQ-loaded micelles at a 1:20 ratio was slightly less efficient, potentially due to reduced accessibility of PDSM groups after IMQ encapsulation, though OVA conjugation remained >80%. Protein release and disulfide bond reversibility, two properties proven to enhance conjugate-based vaccine delivery,[45] was demonstrated through treatment with the reducing agent TCEP. Conjugation results in distributing OVA over a broad range of molecular weights, indicating variation in the number of OVA conjugated per polymer chain.[43] The hydrodynamic diameter of conjugates were analyzed by DLS, revealing no significant change in size (35.5 $\pm$ 0.1 nm OVA-LMA50 and 34.0 $\pm$ 0.3 nm OVA-LMA50-IMQ), which signifies negligible particle cross-linking or aggregation.

To initiate adaptive cellular immunity, antigens must be first be internalized by professional APCs and subsequently processed and presented as peptide epitopes on MHC for recognition by T cells. Based on the well-established proclivity of macrophages and DCs for endocytosis of micro- and nanoparticles,[83] we postulated that conjugation of OVA to the micelle corona would enhance antigen internalization. To evaluate this, OVA488 was conjugated to LMA50 micelles, with and without IMQ, and flow cytometry was used to measure uptake relative to free OVA488 (Figure 5B, C). Conjugation of OVA488 to empty LMA50 micelles resulted in a significant, but only modest increase in OVA488 uptake, a likely consequence of the highly PEGylated, stealth-like micelle corona. Strikingly, OVA488 with IMQ-loaded micelles resulted in a 4-fold increase in OVA488 uptake relative to free antigen (Figure 5B). We speculate that the increased OVA488 uptake was a consequence of the enhanced immunostimulatory activity of micellar IMQ formulations, as TLR activation acutely stimulates macropinocytosis by DCs,[84] a common mechanism of nanoparticle uptake. Even though DC maturation typically down-regulates endocytic capacity, this effect may be TLR-specific, as DC phagocytic activity is maintained after TLR7/8 activation.[85] To evaluate the ability of micelles to enhance delivery of a hydrophobic drug, we used a model hydrophobic molecule, NR, as a fluorescent analogue of IMQ to monitor internalization by flow cytometry. Similarly, OVA488-LMA50-NR revealed 12-fold higher levels of cell-associated NR relative to incubation with the free dye (Figure 5C). Taken together, these results underscore the importance of particle-based carriers to enhance the intracellular delivery of both antigens and water insoluble, hydrophobic compounds.

Dual Delivery of Antigen and IMQ Enhances MHC-I Presentation. The predominant fate of endocytosed soluble antigen is lysosomal degradation and presentation by MHC-II molecules and minimal presentation on MHC-I (i.e., cross-presentation), resulting in negligible $CD8^+$ T cell responses. That notwithstanding, TLR agonists, including IMQ,[86,87] as well as a number of particle-based carriers[83] have been shown to enhance antigen cross-presentation. DC2.4 cells, a dendritic cell line derived from BMDCs, are capable of cross-presenting exogenous antigen[88] and can also be activated with free or encapsulated IMQ (Figure S16), and therefore were used to investigate the synergistic effects of dual delivery of antigen and adjuvant. To determine the effect of micellar antigen delivery on antigen cross-presentation, we incubated DC2.4 cells with

DOI: 10.1021/acsbiomaterials.6b00408
ACS Biomater. Sci. Eng. 2017, 3, 179–194

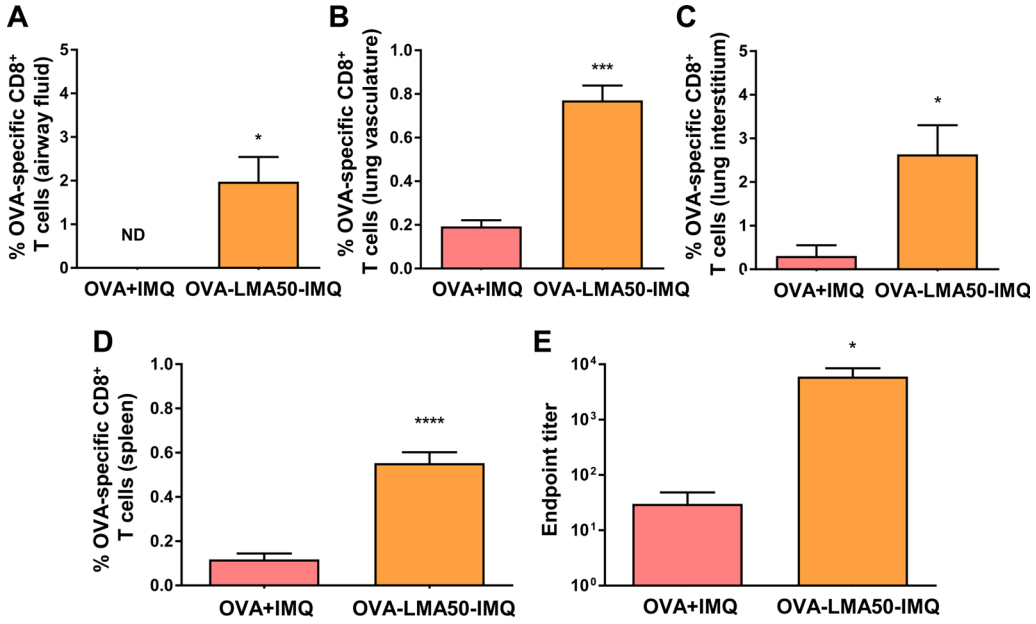

Figure 6. IN vaccination with OVA and IMQ-loaded micelles enhances antigen-specific $CD8^+$ T cell and IgG antibody responses. Mice were vaccinated i.n. with either OVA-LMA50-IMQ carriers or a soluble OVA+IMQ formulation. Mice were sacrificed on day 12 after treatment and frequencies of OVA-specific $CD8^+$ T cells in the (A) broncheoalveolar lavage fluid (BAL: $Tetramer^+$ anti-$CD45^-$), (B) lung vasculature (lung parenchyma: $Tetramer^+$ i.v. anti-$CD45^+$), (C) lung interstitium (lung parenchyma: $Tetramer^+$ i.v. anti-$CD45^-$), and (D) spleen were assessed using intravascular (in vivo) $CD45^+$ staining coupled with ex vivo SIINFEKL-H-$2K^b$ tetramer staining. (E) OVA-specific IgG antibody titer was measured by ELISA from serum collected on day 10 post immunization. ND: not detectable.

free OVA, OVA-LMA50 conjugates with or without IMQ, and a physical mixture of OVA and IMQ. I*n vitro* presentation of the immunodominant MHC-I restricted OVA epitope (SIINFEKL) was assessed by flow cytometry using an antibody that recognizes MHC-I (H-$2K^b$)-bound SIINFEKL. Conjugation of OVA to micelles modestly enhanced cross-presentation (Figure 5D), consistent with enhancement in uptake via a carrier that lacks an active mechanism to enhance cytosolic delivery to the classical class I pathway.[43] Significantly, dual delivery of OVA and IMQ using LMA50 micelles enhanced SIINFEKL presentation by class I molecules by 3-fold over free antigen, 2.5-fold over OVA-LMA50 conjugates, and 2-fold over OVA+IMQ mixture (Figure 5D). This is consistent with the observed micelle-mediated enhancements in IMQ activity as well as increased antigen uptake, indicating a potential synergism via delivery of both antigen and IMQ using fatty acid-mimetic micelles.

Intranasal Immunization with Antigen and IMQ-Loaded Micelles Enhances $CD8^+$ T cell and Antibody Responses. Many pathogens enter the body through mucosal tissues and optimal protection against infection often requires mucosal immune responses localized at the site of infection.[89,90] Most clinically administered vaccines and administration routes (e.g., intramuscular) rarely induce mucosal immunity.[91] This challenge has motivated interest in the development of mucosal vaccination approaches, particularly pulmonary immunization via needle-free aerosol or i.n. delivery. On the basis of the ability of IMQ-loaded micelles to enhance DC maturation and pro-inflammatory cytokine production and promote antigen cross-presentation, as well as previous reports describing use of IMQ as a vaccine adjuvant to enhance cellular and humoral immunity, we hypothesized that micellar delivery of IMQ could enhance the immunogenicity of OVA delivered via an i.n. route.

To test this hypothesis, we i.n. vaccinated mice either with a mixture of soluble OVA and IMQ (OVA+IMQ) or with a micelle vaccine comprising encapsulated IMQ and conjugated OVA (OVA-LMA50-IMQ). Doses of IMQ (10 μg) and OVA (40 μg) were equivalent in both formulations, though an acidic media (0.1 M HEPES containing 0.1 M lactic acid, pH ~3) was required to solubilize IMQ in a soluble formulation. After 12 days, the frequency of pulmonary and splenic SIINFEKL-specific $CD8^+$ T cells was quantified after staining with SIINFEKL-H-$2K^b$ tetramer (Tet). Additionally, to distinguish $CD8^+$ T cells residing in the distinct lung compartments, such as vasculature, interstitium, and airways, we utilized an in vivo CD45 staining technique as described previously (Figures S17–19).[92] Immunization with the soluble formulation did not elicit a detectable $CD8^+$ T cell response, whereas the micelle formulation induced a modest but significant OVA-specific $CD8^+$ T cell response in all lung compartments and the spleen (Figure 6A–D). Notably, micelle vaccines elicited ~2% OVA-specific airway (BAL fraction: Tet^+ i.v. anti-$CD45^-$) and ~3% interstitial (lung parenchymal fraction: Tet^+ i.v. anti-$CD45^-$) $CD8^+$ T cells, the two populations critical to optimal defense against many intracellular respiratory pathogens (e.g., influenza viruses, Mycobacterium tuberculosis).[90]

Eliciting a $CD8^+$ T cell response to a protein subunit vaccine requires that a cohort of endocytosed antigen be cross-presented by DCs in the context of costimulation. In the lungs, there are two primary DC subsets, $CD103^+$ DCs and $CD11b^+$ DCs, both of which can migrate from the lung to the draining LN to present antigen to T cells.[93] IMQ, and other TLR7 agonists, have been shown to enhance antigen cross presentation in specialized DC subsets,[94] but the role of TLR7 has not been widely explored in the lung. A recent study demonstrated that $CD11b^+$ DCs, which express higher levels of TLR7 than $CD103^+$ DCs, could induce $CD8^+$ T cell responses if activated with the TLR7 agonist R848 (resiquimod) but only if they are also presenting the antigen; i.e., the antigen and adjuvant must be delivered in cis.[95] Whether $CD11b^+$ DCs

DOI: 10.1021/acsbiomaterials.6b00408
ACS Biomater. Sci. Eng. 2017, 3, 179–194

facilitated dual delivery of antigen and IMQ after i.n. vaccination awaits further investigations.

I.n. administration with micellar vaccine formulations also increased serum OVA-specific IgG titers 200-fold over the soluble formulation, which failed to induce a detectable response (Figure 6E). These data suggest that micellar vaccines may also enhance $CD4^+$ T cell responses. Interestingly, analysis of IgG subtypes revealed a significantly higher IgG1 response with negligible IgG2c, indicating a Th2-biased response (Figure S20). This result contrasts previous reports implicating IMQ as a Th1-type adjuvant[19] and as a therapeutic for mitigating Th2-driven allergy and asthma in the airways.[96] The Th2-biased antibody response observed in the study may reflect incomplete or insufficient IgG class switching due to the lack of a booster vaccination and/or the time point at which antibody titers were measured. Indeed, using a nanoparticle-based vaccine loaded with IMQ, a shift in IgG1/IgG2a ratio to less than unity was previously reported following three i.n. vaccinations over 28 weeks.[37] We note that these investigations were directed toward establishing the potential of fatty acid-mimetic micelles as vaccine carriers to elicit cellular and humoral immune responses to protein subunit antigens. Further investigation is necessary to understand the mechanisms by which LMA50 micelles enhance immunogenicity and to elucidate the relative contributions of micellar antigen and IMQ delivery in mediating this response. Additional studies are also necessary to further characterize the immune response elicited by this vaccine formulation, including mechanisms of particle trafficking to draining lymph nodes, analysis of germinal center formation, phenotype and functionality of the T cell response, and characterization of immune responses in other mucosal tissues. Nonetheless the enhanced immunogenicity of the nanoparticle-based antigen and adjuvant delivery reported in this proof-of-principle study merits rigorous characterization of the dose and vaccination regimen that optimally elicits mucosal innate and adaptive immunity.

CONCLUSION

We have developed a new class of vaccine based on polymeric nanoparticles that are engineered to enable dual delivery of protein antigens and the small molecule TLR-7 agonist, IMQ. Owing to the preferential solubility of IMQ in fatty acids, we utilized RAFT polymerization to synthesize well-defined amphiphilic diblock copolymers that self-assemble into micelles with a fatty acid-mimetic core for IMQ encapsulation, and a hydrophilic, PEG-rich corona doped with thiol-reactive PDSM groups for covalent antigen conjugation. Encapsulation of IMQ was maximized using an equimolar ratio of hydrophobic lauryl methacrylate and methacrylic acid in the core-forming block. Optimized carriers significantly enhanced the immunostimulatory activity of IMQ, resulting in enhanced cytokine production, costimulatory molecule expression, and antigen cross-presentation by DCs. I.n. vaccination with micellar nanoparticles coloaded with IMQ and a protein antigen resulted in a significantly greater pulmonary antigen-specific $CD8^+$ T cell response and systemic IgG response compared to a soluble formulation of antigen and adjuvant. Even though a model antigen was used and immunization regimens remain to be optimized, the encouraging results reported herein motivate further evaluation of this technology for induction of mucosal cellular immunity and vaccination against respiratory pathogens. Furthermore, because of their small size, highly PEGylated corona, and minimal cytotoxicity, fatty acid-mimetic micelles may also provide a strategy to overcome the poor pharmacokinetics and systemic toxicity that have limited exploration of IMQ as a systemically administered cancer immunotherapeutic. In conclusion, fatty acid-mimetic micelles represent a versatile new platform for improving the delivery and activity of IMQ, thereby expanding its potential use and efficacy as an antiviral agent, cancer immunotherapeutic, and vaccine adjuvant.

ASSOCIATED CONTENT

Supporting Information

The Supporting Information is available free of charge on the ACS Publications website at DOI: 10.1021/acsbiomaterials.6b00408.

Figures S1−S20, Schemes S1 and S2, and Table S1 (PDF)

AUTHOR INFORMATION

Corresponding Author

*E-mail: john.t.wilson@vanderbilt.edu. Tel: +1-615-322-6406.

Notes

The authors declare no competing financial interest.

ACKNOWLEDGMENTS

We gratefully acknowledge the laboratory of Prof. Craig Duvall for the use of GPC as well as the core facilities of the Vanderbilt Institute of Nanoscale Science and Engineering (VINSE) for the use of both the DLS and TEM instruments. We also acknowledge the VUMC Flow Cytometry Shared Resources, supported by the Vanderbilt Ingram Cancer Center (P30 CA68485) and the Vanderbilt Digestive Disease Research Center (DK058404), for the usage of 3-laser BD LSRII flow cytometery. This research was supported by NSF CAREER Award CBET 1554623 (J.T.W.), NIH 1R21AI121626-01A1 (J.T.W.), the Vanderbilt University Discovery Grant Program (J.T.W.), and the Vanderbilt University School of Engineering (J.T.W.). S.J. acknowledges the U.S. Department of Veterans Affairs for the Merit Award (BX001444).

REFERENCES

(1) Rappuoli, R.; Aderem, A. A 2020 vision for vaccines against HIV, tuberculosis and malaria. *Nature* **2011**, *473* (7348), 463−9.
(2) Nabel, G. J. Designing tomorrow's vaccines. *N. Engl. J. Med.* **2013**, *368* (6), 551−60.
(3) Reed, S. G.; Orr, M. T.; Fox, C. B. Key roles of adjuvants in modern vaccines. *Nat. Med.* **2013**, *19* (12), 1597−608.
(4) Coffman, R. L.; Sher, A.; Seder, R. A. Vaccine Adjuvants: Putting Innate Immunity to Work. *Immunity* **2010**, *33* (4), 492−503.
(5) Perrie, Y.; Mohammed, A. R.; Kirby, D. J.; McNeil, S. E.; Bramwell, V. W. Vaccine adjuvant systems: enhancing the efficacy of sub-unit protein antigens. *Int. J. Pharm.* **2008**, *364* (2), 272−80.
(6) Marrack, P.; McKee, A. S.; Munks, M. W. Towards an understanding of the adjuvant action of aluminium. *Nat. Rev. Immunol.* **2009**, *9* (4), 287−93.
(7) Yewdell, J. W. Designing CD8+ T cell vaccines: it's not rocket science (yet). *Curr. Opin. Immunol.* **2010**, *22* (3), 402−10.
(8) Foged, C.; Hansen, J.; Agger, E. M. License to kill: Formulation requirements for optimal priming of CD8(+) CTL responses with particulate vaccine delivery systems. *Eur. J. Pharm. Sci.* **2012**, *45* (4), 482−91.
(9) Mount, A.; Koernig, S.; Silva, A.; Drane, D.; Maraskovsky, E.; Morelli, A. B. Combination of adjuvants: the future of vaccine design. *Expert Rev. Vaccines* **2013**, *12* (7), 733−46.

DOI: 10.1021/acsbiomaterials.6b00408
ACS Biomater. Sci. Eng. 2017, 3, 179−194

(10) Iwasaki, A.; Medzhitov, R. Toll-like receptor control of the adaptive immune responses. *Nat. Immunol.* **2004**, *5* (10), 987−995.
(11) Broz, P.; Monack, D. M. Newly described pattern recognition receptors team up against intracellular pathogens. *Nat. Rev. Immunol.* **2013**, *13* (8), 551−65.
(12) Kawai, T.; Akira, S. The role of pattern-recognition receptors in innate immunity: update on Toll-like receptors. *Nat. Immunol.* **2010**, *11* (5), 373−84.
(13) Toussi, D. N.; Massari, P. Immune Adjuvant Effect of Molecularly-defined Toll-Like Receptor Ligands. *Vaccines (Basel, Switz.)* **2014**, *2* (2), 323−53.
(14) Cheever, M. A. Twelve immunotherapy drugs that could cure cancers. *Immunol. Rev.* **2008**, *222*, 357−68.
(15) Lund, J. M.; Alexopoulou, L.; Sato, A.; Karow, M.; Adams, N. C.; Gale, N. W.; Iwasaki, A.; Flavell, R. A. Recognition of single-stranded RNA viruses by Toll-like receptor 7. *Proc. Natl. Acad. Sci. U. S. A.* **2004**, *101* (15), 5598−5603.
(16) Hemmi, H.; Kaisho, T.; Takeuchi, O.; Sato, S.; Sanjo, H.; Hoshino, K.; Horiuchi, T.; Tomizawa, H.; Takeda, K.; Akira, S. Small anti-viral compounds activate immune cells via the TLR7MyD88-dependent signaling pathway. *Nat. Immunol.* **2002**, *3* (2), 196−200.
(17) Othoro, C.; Johnston, D.; Lee, R.; Soverow, J.; Bystryn, J.-C.; Nardin, E. Enhanced Immunogenicity of Plasmodium falciparum Peptide Vaccines Using a Topical Adjuvant Containing a Potent Synthetic Toll-Like Receptor 7 Agonist, Imiquimod. *Infect. Immun.* **2009**, *77* (2), 739−748.
(18) Lynn, G. M.; Laga, R.; Darrah, P. A.; Ishizuka, A. S.; Balaci, A. J.; Dulcey, A. E.; Pechar, M.; Pola, R.; Gerner, M. Y.; Yamamoto, A.; Buechler, C. R.; Quinn, K. M.; Smelkinson, M. G.; Vanek, O.; Cawood, R.; Hills, T.; Vasalatiy, O.; Kastenmuller, K.; Francica, J. R.; Stutts, L.; Tom, J. K.; Ryu, K. A.; Esser-Kahn, A. P.; Etrych, T.; Fisher, K. D.; Seymour, L. W.; Seder, R. A. In vivo characterization of the physicochemical properties of polymer-linked TLR agonists that enhance vaccine immunogenicity. *Nat. Biotechnol.* **2015**, *33* (11), 1201−1210.
(19) Vasilakos, J. P.; Tomai, M. A. The use of Toll-like receptor 7/8 agonists as vaccine adjuvants. *Expert Rev. Vaccines* **2013**, *12* (7), 809−19.
(20) Hanna, E.; Abadi, R.; Abbas, O. Imiquimod in dermatology: an overview. *Int. J. Dermatol.* **2016**, *55* (8), 831−44.
(21) Chollet, J.; Jozwiakowski, M.; Phares, K.; Reiter, M.; Roddy, P.; Schultz, H.; Ta, Q.; Tomai, M. Development of a Topically Active Imiquimod Formulation. *Pharm. Dev. Technol.* **1999**, *4* (1), 35.
(22) Soria, I.; Myhre, P.; Horton, V.; Ellefson, P.; McCarville, S.; Schmitt, K.; Owens, M. Effect of food on the pharmacokinetics and bioavailability of oral imiquimod relative to a subcutaneous dose. *Int. J. Clin. Pharmacol. Ther.* **2000**, *38* (10), 476−81.
(23) Nuhn, L.; Vanparijs, N.; De Beuckelaer, A.; Lybaert, L.; Verstraete, G.; Deswarte, K.; Lienenklaus, S.; Shukla, N. M.; Salyer, A. C.; Lambrecht, B. N.; Grooten, J.; David, S. A.; De Koker, S.; De Geest, B. G. pH-degradable imidazoquinoline-ligated nanogels for lymph node-focused immune activation. *Proc. Natl. Acad. Sci. U. S. A.* **2016**, *113*, 8098.
(24) Dudek, A. Z.; Yunis, C.; Harrison, L. I.; Kumar, S.; Hawkinson, R.; Cooley, S.; Vasilakos, J. P.; Gorski, K. S.; Miller, J. S. First in human phase I trial of 852A, a novel systemic toll-like receptor 7 agonist, to activate innate immune responses in patients with advanced cancer. *Clin. Cancer Res.* **2007**, *13* (23), 7119−25.
(25) Savage, P.; Horton, V.; Moore, J.; Owens, M.; Witt, P.; Gore, M. E. A phase I clinical trial of imiquimod, an oral interferon inducer, administered daily. *Br. J. Cancer* **1996**, *74* (9), 1482−1486.
(26) Schon, M. P.; Schon, M. TLR7 and TLR8 as targets in cancer therapy. *Oncogene* **2008**, *27* (2), 190−199.
(27) Pockros, P. J.; Guyader, D.; Patton, H.; Tong, M. J.; Wright, T.; McHutchison, J. G.; Meng, T.-C. Oral resiquimod in chronic HCV infection: Safety and efficacy in 2 placebo-controlled, double-blind phase IIa studies. *J. Hepatol.* **2007**, *47* (2), 174−182.
(28) Wu, T. Y.; Singh, M.; Miller, A. T.; De Gregorio, E.; Doro, F.; D'Oro, U.; Skibinski, D. A.; Mbow, M. L.; Bufali, S.; Herman, A. E.; Cortez, A.; Li, Y.; Nayak, B. P.; Tritto, E.; Filippi, C. M.; Otten, G. R.; Brito, L. A.; Monaci, E.; Li, C.; Aprea, S.; Valentini, S.; Calabro, S.; Laera, D.; Brunelli, B.; Caproni, E.; Malyala, P.; Panchal, R. G.; Warren, T. K.; Bavari, S.; O'Hagan, D. T.; Cooke, M. P.; Valiante, N. M. Rational design of small molecules as vaccine adjuvants. *Sci. Transl. Med.* **2014**, *6* (263), 263ra160.
(29) Bachelder, E. M.; Beaudette, T. T.; Broaders, K. E.; Fréchet, J. M. J.; Albrecht, M. T.; Mateczun, A. J.; Ainslie, K. M.; Pesce, J. T.; Keane-Myers, A. M. In Vitro Analysis of Acetalated Dextran Microparticles as a Potent Delivery Platform for Vaccine Adjuvants. *Mol. Pharmaceutics* **2010**, *7* (3), 826−835.
(30) Primard, C.; Poecheim, J.; Heuking, S.; Sublet, E.; Esmaeili, F.; Borchard, G. Multifunctional PLGA-Based Nanoparticles Encapsulating Simultaneously Hydrophilic Antigen and Hydrophobic Immunomodulator for Mucosal Immunization. *Mol. Pharmaceutics* **2013**, *10* (8), 2996−3004.
(31) Kasturi, S. P.; Skountzou, I.; Albrecht, R. A.; Koutsonanos, D.; Hua, T.; Nakaya, H. I.; Ravindran, R.; Stewart, S.; Alam, M.; Kwissa, M.; Villinger, F.; Murthy, N.; Steel, J.; Jacob, J.; Hogan, R. J.; Garcia-Sastre, A.; Compans, R.; Pulendran, B. Programming the magnitude and persistence of antibody responses with innate immunity. *Nature* **2011**, *470* (7335), 543−7.
(32) Seth, A.; Heo, M. B.; Lim, Y. T. Poly (γ-glutamic acid) based combination of water-insoluble paclitaxel and TLR7 agonist for chemo-immunotherapy. *Biomaterials* **2014**, *35* (27), 7992−8001.
(33) Wilson, J. T.; Keller, S.; Manganiello, M. J.; Cheng, C.; Lee, C.-C.; Opara, C.; Convertine, A.; Stayton, P. S. pH-Responsive Nanoparticle Vaccines for Dual-Delivery of Antigens and Immunostimulatory Oligonucleotides. *ACS Nano* **2013**, *7* (5), 3912−3925.
(34) Moon, J. J.; Suh, H.; Bershteyn, A.; Stephan, M. T.; Liu, H.; Huang, B.; Sohail, M.; Luo, S.; Um, S. H.; Khant, H.; Goodwin, J. T.; Ramos, J.; Chiu, W.; Irvine, D. J. Interbilayer-crosslinked multilamellar vesicles as synthetic vaccines for potent humoral and cellular immune responses. *Nat. Mater.* **2011**, *10* (3), 243−51.
(35) Chiu, Y. C.; Gammon, J. M.; Andorko, J. I.; Tostanoski, L. H.; Jewell, C. M. Modular Vaccine Design Using Carrier-Free Capsules Assembled from Polyionic Immune Signals. *ACS Biomater. Sci. Eng.* **2015**, *1* (12), 1200−1205.
(36) Rizwan, S. B.; McBurney, W. T.; Young, K.; Hanley, T.; Boyd, B. J.; Rades, T.; Hook, S. Cubosomes containing the adjuvants imiquimod and monophosphoryl lipid A stimulate robust cellular and humoral immune responses. *J. Controlled Release* **2013**, *165* (1), 16−21.
(37) Vicente, S.; Peleteiro, M.; Díaz-Freitas, B.; Sanchez, A.; González-Fernández, Á.; Alonso, M. J. Co-delivery of viral proteins and a TLR7 agonist from polysaccharide nanocapsules: A needle-free vaccination strategy. *J. Controlled Release* **2013**, *172* (3), 773−781.
(38) Heo, M. B.; Lim, Y. T. Programmed nanoparticles for combined immunomodulation, antigen presentation and tracking of immunotherapeutic cells. *Biomaterials* **2014**, *35* (1), 590−600.
(39) Reddy, S. T.; van der Vlies, A. J.; Simeoni, E.; Angeli, V.; Randolph, G. J.; O'Neil, C. P.; Lee, L. K.; Swartz, M. A.; Hubbell, J. A. Exploiting lymphatic transport and complement activation in nanoparticle vaccines. *Nat. Biotechnol.* **2007**, *25* (10), 1159−64.
(40) Fang, J.; Nakamura, H.; Maeda, H. The EPR effect: Unique features of tumor blood vessels for drug delivery, factors involved, and limitations and augmentation of the effect. *Adv. Drug Delivery Rev.* **2011**, *63* (3), 136−151.
(41) Bilati, U.; Allemann, E.; Doelker, E. Strategic approaches for overcoming peptide and protein instability within biodegradable nano- and microparticles. *Eur. J. Pharm. Biopharm.* **2005**, *59* (3), 375−88.
(42) Fox, C. B.; Sivananthan, S. J.; Duthie, M. S.; Vergara, J.; Guderian, J. A.; Moon, E.; Coblentz, D.; Reed, S. G.; Carter, D. A nanoliposome delivery system to synergistically trigger TLR4 AND TLR7. *J. Nanobiotechnol.* **2014**, *12*, 17.
(43) Keller, S.; Wilson, J. T.; Patilea, G. I.; Kern, H. B.; Convertine, A. J.; Stayton, P. S. Neutral polymer micelle carriers with pH-responsive, endosome-releasing activity modulate antigen trafficking to

DOI: 10.1021/acsbiomaterials.6b00408
ACS Biomater. Sci. Eng. 2017, 3, 179−194

enhance CD8+ T cell responses. *J. Controlled Release* **2014**, *191*, 24−33.
(44) Wilson, J. T.; Postma, A.; Keller, S.; Convertine, A. J.; Moad, G.; Rizzardo, E.; Meagher, L.; Chiefari, J.; Stayton, P. S. Enhancement of MHC-I antigen presentation via architectural control of pH-responsive, endosomolytic polymer nanoparticles. *AAPS J.* **2015**, *17* (2), 358−69.
(45) Hirosue, S.; Kourtis, I. C.; van der Vlies, A. J.; Hubbell, J. A.; Swartz, M. A. Antigen delivery to dendritic cells by poly(propylene sulfide) nanoparticles with disulfide conjugated peptides: Cross-presentation and T cell activation. *Vaccine* **2010**, *28* (50), 7897−7906.
(46) Moad, G. RAFT Polymerization − Then and Now. In *Controlled Radical Polymerization: Mechanisms*; American Chemical Society: Washington, D.C., 2015; Vol. *1187*, pp 211−246; DOI: 10.1021/bk-2015-1187.ch012.
(47) Moad, G.; Rizzardo, E.; Thang, S. H. Living Radical Polymerization by the RAFT Process. *Aust. J. Chem.* **2005**, *58* (6), 379−410.
(48) Wong, L. J.; Sevimli, S.; Zareie, H. M.; Davis, T. P.; Bulmus, V. PEGylated Functional Nanoparticles from a Reactive Homopolymer Scaffold Modified by Thiol Addition Chemistry. *Macromolecules* **2010**, *43* (12), 5365−5375.
(49) Wong, L. J.; Boyer, C.; Jia, Z. F.; Zareie, H. M.; Davis, T. P.; Bulmus, V. Synthesis of versatile thiol-reactive polymer scaffolds via RAFT polymerization. *Biomacromolecules* **2008**, *9* (7), 1934−1944.
(50) Kurniasih, I. N.; Liang, H.; Mohr, P. C.; Khot, G.; Rabe, J. P.; Mohr, A. Nile Red Dye in Aqueous Surfactant and Micellar Solution. *Langmuir* **2015**, *31* (9), 2639−2648.
(51) Gupta, M. K.; Meyer, T. A.; Nelson, C. E.; Duvall, C. L. Poly(PS-b-DMA) Micelles for Reactive Oxygen Species Triggered Drug Release. *J. Controlled Release* **2012**, *162* (3), 591−598.
(52) Sevimli, S.; Sagnella, S.; Kavallaris, M.; Bulmus, V.; Davis, T. P. Synthesis, self-assembly and stimuli responsive properties of cholesterol conjugated polymers. *Polym. Chem.* **2012**, *3* (8), 2057−2069.
(53) Porgador, A.; Yewdell, J. W.; Deng, Y.; Bennink, J. R.; Germain, R. N. Localization, Quantitation, and In Situ Detection of Specific Peptide−MHC Class I Complexes Using a Monoclonal Antibody. *Immunity* **1997**, *6* (6), 715−726.
(54) Brito, L. A.; Singh, M. COMMENTARY: Acceptable Levels of Endotoxin in Vaccine Formulations During Preclinical Research. *J. Pharm. Sci.* **2011**, *100* (1), 34−37.
(55) Gilchuk, P.; Knight, F. C.; Wilson, J. T.; Joyce, S. Eliciting Epitope-Specific CD8+ T Cell Response by Immunization with Microbial Protein Antigens Formulated with alpha-Galactosylceramide: Theory, Practice, and Protocols. In *Vaccine Adjuvants: Methods and Protocols*; Fox, C. B., Ed.; Methods in Molecular Biology; Springer: New York, 2017; pp 321−352.
(56) Rodenko, B.; Toebes, M.; Hadrup, S. R.; van Esch, W. J. E.; Molenaar, A. M.; Schumacher, T. N. M.; Ovaa, H. Generation of peptide-MHC class I complexes through UV-mediated ligand exchange. *Nat. Protoc.* **2006**, *1* (3), 1120−1132.
(57) Sevimli, S.; Inci, F.; Zareie, H. M.; Bulmus, V. Well-Defined Cholesterol Polymers with pH-Controlled Membrane Switching Activity. *Biomacromolecules* **2012**, *13* (10), 3064−3075.
(58) Gao, W.; Liu, W.; Christensen, T.; Zalutsky, M. R.; Chilkoti, A. In situ growth of a PEG-like polymer from the C terminus of an intein fusion protein improves pharmacokinetics and tumor accumulation. *Proc. Natl. Acad. Sci. U. S. A.* **2010**, *107* (38), 16432−7.
(59) Berguig, G. Y.; Convertine, A. J.; Frayo, S.; Kern, H. B.; Procko, E.; Roy, D.; Srinivasan, S.; Margineantu, D. H.; Booth, G.; Palanca-Wessels, M. C.; Baker, D.; Hockenbery, D.; Press, O. W.; Stayton, P. S. Intracellular delivery system for antibody-Peptide drug conjugates. *Mol. Ther.* **2015**, *23* (5), 907−17.
(60) Foster, S.; Duvall, C. L.; Crownover, E. F.; Hoffman, A. S.; Stayton, P. S. Intracellular Delivery of a Protein Antigen with an Endosomal-Releasing Polymer Enhances CD8 T-Cell Production and Prophylactic Vaccine Efficacy. *Bioconjugate Chem.* **2010**, *21* (12), 2205−2212.
(61) Kilian, L.; Wang, Z.-H.; Long, T. E. Synthesis and cleavage of core-labile poly(alkyl methacrylate) star polymers. *J. Polym. Sci., Part A: Polym. Chem.* **2003**, *41* (19), 3083−3093.
(62) Lee, S. C.; Kim, K. J.; Jeong, Y.-K.; Chang, J. H.; Choi, J. pH-Induced Reversible Complexation of Poly(ethylene glycol) and Poly(ε-caprolactone)-b-poly(methacrylic acid) Copolymer Micelles. *Macromolecules* **2005**, *38* (22), 9291−9297.
(63) Mengel, C.; Meyer, W. H.; Wegner, G. Photocrosslinkable Star Polymers: Precursors for Model Polyelectrolyte Networks. *Macromol. Chem. Phys.* **2001**, *202* (7), 1138−1149.
(64) Ong, J. T.; Manoukian, E. Micellar solubilization of timobesone acetate in aqueous and aqueous propylene glycol solutions of nonionic surfactants. *Pharm. Res.* **1988**, *5* (11), 704−708.
(65) Kim, Y.; Pourgholami, M. H.; Morris, D. L.; Stenzel, M. H. An Optimized RGD-Decorated Micellar Drug Delivery System for Albendazole for the Treatment of Ovarian Cancer: From RAFT Polymer Synthesis to Cellular Uptake. *Macromol. Biosci.* **2011**, *11* (2), 219−233.
(66) Jiang, X.; Zhao, B. Tuning Micellization and Dissociation Transitions of Thermo- and pH-Sensitive Poly(ethylene oxide)-b-poly(methoxydi(ethylene glycol) methacrylate-co-methacrylic acid) in Aqueous Solution by Combining Temperature and pH Triggers. *Macromolecules* **2008**, *41* (23), 9366−9375.
(67) Zhou, Y.; Briand, V.; Sharma, N.; Ahn, S.-k.; Kasi, R. Polymers Comprising Cholesterol: Synthesis, Self-Assembly, and Applications. *Materials* **2009**, *2* (2), 636.
(68) Cobo Sánchez, C.; Wåhlander, M.; Taylor, N.; Fogelström, L.; Malmström, E. Novel Nanocomposites of Poly(lauryl methacrylate)-Grafted Al2O3 Nanoparticles in LDPE. *ACS Appl. Mater. Interfaces* **2015**, *7* (46), 25669−25678.
(69) Convertine, A. J.; Diab, C.; Prieve, M.; Paschal, A.; Hoffman, A. S.; Johnson, P. H.; Stayton, P. S. pH-Responsive Polymeric Micelle Carriers for siRNA Drugs. *Biomacromolecules* **2010**, *11* (11), 2904−2911.
(70) Topel, Ö.; Çakır, B. A.; Budama, L.; Hoda, N. Determination of critical micelle concentration of polybutadiene-block-poly(ethyleneoxide) diblock copolymer by fluorescence spectroscopy and dynamic light scattering. *J. Mol. Liq.* **2013**, *177*, 40−43.
(71) Zhang, A.; Zhang, Z.; Shi, F.; Ding, J.; Xiao, C.; Zhuang, X.; He, C.; Chen, L.; Chen, X. Disulfide crosslinked PEGylated starch micelles as efficient intracellular drug delivery platforms. *Soft Matter* **2013**, *9* (7), 2224−2233.
(72) Chen, C.; Liu, G.; Liu, X.; Pang, S.; Zhu, C.; Lv, L.; Ji, J. Photo-responsive, biocompatible polymeric micelles self-assembled from hyperbranched polyphosphate-based polymers. *Polym. Chem.* **2011**, *2* (6), 1389−1397.
(73) Trivedi, R.; Kompella, U. B. Nanomicellar formulations for sustained drug delivery: strategies and underlying principles. *Nanomedicine (London, U. K.)* **2010**, *5* (3), 485−505.
(74) Handké, N.; Lahaye, V.; Bertin, D.; Delair, T.; Verrier, B.; Gigmes, D.; Trimaille, T. Elaboration of Glycopolymer-Functionalized Micelles from an N-Vinylpyrrolidone/Lactide-Based Reactive Copolymer Platform. *Macromol. Biosci.* **2013**, *13* (9), 1213−1220.
(75) Chen, C.-Y.; Kim, T. H.; Wu, W.-C.; Huang, C.-M.; Wei, H.; Mount, C. W.; Tian, Y.; Jang, S.-H.; Pun, S. H.; Jen, A. K. Y. pH-dependent, thermosensitive polymeric nanocarriers for drug delivery to solid tumors. *Biomaterials* **2013**, *34* (18), 4501−4509.
(76) Manesiotis, P.; Kashani, S.; McLoughlin, P. Molecularly imprinted polymers for the extraction of imiquimod from biological samples using a template analogue strategy. *Anal. Methods* **2013**, *5* (12), 3122−3128.
(77) Kanamala, M.; Wilson, W. R.; Yang, M.; Palmer, B. D.; Wu, Z. Mechanisms and biomaterials in pH-responsive tumour targeted drug delivery: A review. *Biomaterials* **2016**, *85*, 152−67.
(78) Jiménez-Sánchez, G.; Pavot, V.; Chane-Haong, C.; Handké, N.; Terrat, C.; Gigmes, D.; Trimaille, T.; Verrier, B. Preparation and In Vitro Evaluation of Imiquimod Loaded Polylactide-based Micelles as Potential Vaccine Adjuvants. *Pharm. Res.* **2015**, *32*, 311−320.

DOI: 10.1021/acsbiomaterials.6b00408
ACS Biomater. Sci. Eng. 2017, 3, 179−194

(79) Handké, N.; Trimaille, T.; Luciani, E.; Rollet, M.; Delair, T.; Verrier, B.; Bertin, D.; Gigmes, D. Elaboration of densely functionalized polylactide nanoparticles from N-acryloxysuccinimide-based block copolymers. *J. Polym. Sci., Part A: Polym. Chem.* **2011**, *49* (6), 1341−1350.
(80) Ma, F.; Zhang, J.; Zhang, J.; Zhang, C. The TLR7 agonists imiquimod and gardiquimod improve DC-based immunotherapy for melanoma in mice. *Cell. Mol. Immunol.* **2010**, *7* (5), 381−388.
(81) Testerman, T. L.; Gerster, J. F.; Imbertson, L. M.; Reiter, M. J.; Miller, R. L.; Gibson, S. J.; Wagner, T. L.; Tomai, M. A. Cytokine induction by the immunomodulators imiquimod and S-27609. *J. Leukocyte Biol.* **1995**, *58* (3), 365−372.
(82) Fothergill, L. A.; Fothergill, J. E. Thiol and disulphide contents of hen ovalbumin. C-Terminal sequence and location of disulphide bond. *Biochem. J.* **1970**, *116* (4), 555−561.
(83) Moon, J. J.; Huang, B.; Irvine, D. J. Engineering Nano- and Microparticles to Tune Immunity. *Adv. Mater.* **2012**, *24* (28), 3724−3746.
(84) Watts, C.; West, M. A.; Zaru, R. TLR signalling regulated antigen presentation in dendritic cells. *Curr. Opin. Immunol.* **2010**, *22* (1), 124−30.
(85) Weck, M. M.; Grunebach, F.; Werth, D.; Sinzger, C.; Bringmann, A.; Brossart, P. TLR ligands differentially affect uptake and presentation of cellular antigens. *Blood* **2007**, *109* (9), 3890−4.
(86) Chang, B. A.; Cross, J. L.; Najar, H. M.; Dutz, J. P. Topical resiquimod promotes priming of CTL to parenteral antigens. *Vaccine* **2009**, *27* (42), 5791−9.
(87) Oh, J. Z.; Kedl, R. M. The capacity to induce cross-presentation dictates the success of a TLR7 agonist-conjugate vaccine for eliciting cellular immunity. *J. Immunol.* **2010**, *185* (8), 4602−8.
(88) Shen, Z.; Reznikoff, G.; Dranoff, G.; Rock, K. L. Cloned dendritic cells can present exogenous antigens on both MHC class I and class II molecules. *J. Immunol.* **1997**, *158* (6), 2723−2730.
(89) Cauley, L. S.; Lefrancois, L. Guarding the perimeter: protection of the mucosa by tissue-resident memory T cells. *Mucosal Immunol.* **2013**, *6* (1), 14−23.
(90) Chiu, C.; Openshaw, P. J. Antiviral B cell and T cell immunity in the lungs. *Nat. Immunol.* **2015**, *16* (1), 18−26.
(91) Woodrow, K. A.; Bennett, K. M.; Lo, D. D. Mucosal vaccine design and delivery. *Annu. Rev. Biomed. Eng.* **2012**, *14*, 17−46.
(92) Gilchuk, P.; Hill, T.; Guy, C.; McMaster, S.; Boyd, K.; Rabacal, W.; Lu, P.; Shyr, Y.; Kohlmeier, J.; Sebzda, E.; Green, D.; Joyce, S. A distinct lung interstitium-resident memory CD8+ T cell subset confers enhanced protection to lower respiratory tract infection. *Cell Rep.* **2016**, *16* (7), 1800−1809.
(93) Plantinga, M.; Hammad, H.; Lambrecht, B. N. Origin and functional specializations of DC subsets in the lung. *Eur. J. Immunol.* **2010**, *40* (8), 2112−8.
(94) Oh, J. Z.; Kurche, J. S.; Burchill, M. A.; Kedl, R. M. TLR7 enables cross-presentation by multiple dendritic cell subsets through a type I IFN-dependent pathway. *Blood* **2011**, *118* (11), 3028−38.
(95) Desch, A. N.; Gibbings, S. L.; Clambey, E. T.; Janssen, W. J.; Slansky, J. E.; Kedl, R. M.; Henson, P. M.; Jakubzick, C. Dendritic cell subsets require cis-activation for cytotoxic CD8 T-cell induction. *Nat. Commun.* **2014**, *5*, 4674.
(96) Drake, M. G.; Kaufman, E. H.; Fryer, A. D.; Jacoby, D. B. The therapeutic potential of Toll-like receptor 7 stimulation in asthma. *Inflammation Allergy: Drug Targets* **2012**, *11* (6), 484−491.

DOI: 10.1021/acsbiomaterials.6b00408
ACS Biomater. Sci. Eng. 2017, 3, 179−194